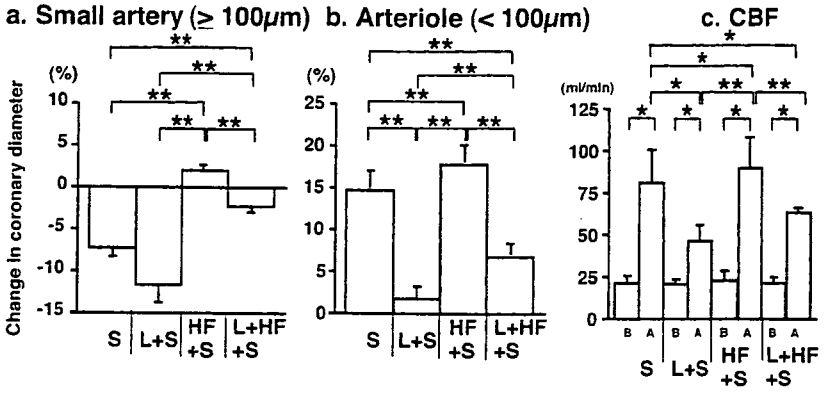


**Figure 3.** Effects of hydroxyfasudil on serotonin-induced coronary vascular responses in dogs in vivo. Hydroxyfasudil converted the serotonin-induced vasoconstriction of small arteries to vasodilation **(a)** and significantly enhanced the serotonin-induced vasodilation of arterioles **(b)**. L-NMMA significantly attenuated the serotonin-induced vasodilation, which was counteracted by hydroxyfasudil. Number of vessels per animal used was 18/6 for S, L + S and HF + S, 13/4 for L + HF + S. *p < 0.05, **p < 0.01. S = serotonin; L = L-NMMA; HF = hydroxyfasudil; B = before drug; A = after drug.

NMMA, Sigma). All drugs were diluted in a physiologic saline immediately before use.

**Statistical analysis.** Results are expressed as means ± SEM. Vascular responses (Figs. 2a to 2c, 3c, 4c, 6c, 7a to 7c, 8a) were analyzed by one-way analysis of variance followed by Scheffe's post-hoc test for multiple comparisons. Difference in the effects of serotonin, acetylcholine, and papaverine on subepicardial microvessels before and after I/R (Figs. 3a, 3b, 4a, 4b, 5a to 5d, 6a, and 6b), and difference between infarct size/risk area and transmural collateral flow with or without hydroxyfasudil (Fig. 8b) were examined by a multiple regression analysis using a model in which the change in coronary diameter was set as a dependent variable (y) and vascular size as an explanatory variable (x) while the statuses of hydroxyfasudil and hydroxyfasudil plus L-NMMA were set as dummy variables ($D_1$, $D_2$) in the following equation; $y = a_0 + a_1x + a_2D_1 + a_3D_2$, where $a_0$ through $a_3$ are partial regression coefficients. The criterion for statistical significance was at $p < 0.05$.

## RESULTS

**Coronary vasodilator effects of hydroxyfasudil.** Intracoronary administration of hydroxyfasudil caused a significant coronary vasodilation of both small arteries and arterioles (Figs. 2a and 2b, both $p < 0.05$, 10 μg/kg vs. 30 and 100 μg/kg) in a dose-dependent manner under control conditions with a resultant increase in CBF (Fig. 2c, $p < 0.05$, C vs. 10, 30 and 100 μg/kg). Intracoronary hydroxyfasudil did not significantly alter mean aortic pressure or heart rate (Table 1).

**Hemodynamics and blood gases during I/R injury.** In each experimental condition, mean aortic pressure and heart rate at baseline were constant and comparable (Table 1), and oxygen partial pressure ($Po_2$), carbon dioxide partial pressure ($Pco_2$), and pH were maintained within the physiologic ranges (pH 7.35 to 7.45, $Pco_2$ 25 to 40 mm Hg, $Po_2$ >70 mm Hg) throughout the experiments. Hemodynamic

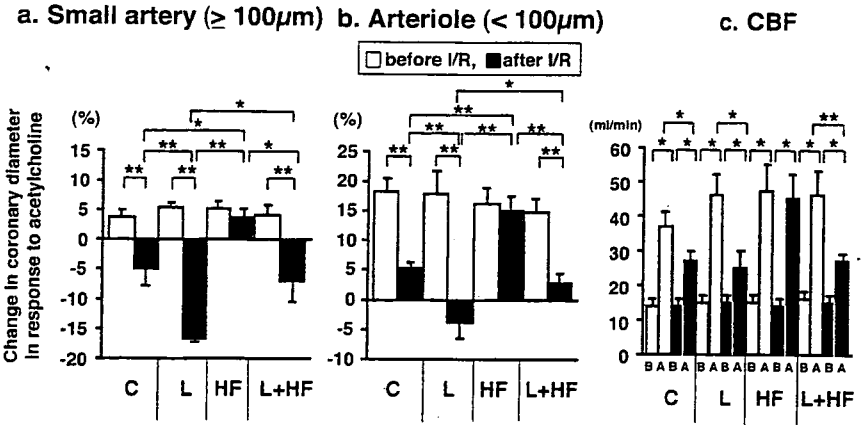


**Figure 4.** Endothelium-dependent coronary vasodilation before and after coronary ischemia/reperfusion (I/R) injury in dogs in vivo. Coronary I/R significantly impaired coronary vasodilation to acetylcholine under control conditions (C) and L-NMMA (L) further suppressed the vasodilation, whereas hydroxyfasudil (HF) completely preserved the responses. The vasoconstriction induced by L-NMMA after I/R was significantly improved by hydroxyfasudil in small arteries. Hydroxyfasudil also prevented the decrease in coronary blood flow (CBF) after I/R, which effect was attenuated by L-NMMA. Number of vessels per animals used was 7/6 for control (mean diameter 120 ± 7 μm), 5/4 for L-NMMA (123 ± 8 μm), 6/4 for hydroxyfasudil (118 ± 8 μm), and 5/4 for hydroxyfasudil plus L-NMMA (125 ± 9 μm) in small arteries, and 12/6 for control (70 ± 6 μm), 8/4 for L-NMMA (69 ± 7 μm), 8/5 for hydroxyfasudil (68 ± 7 μm), and 11/6 for hydroxyfasudil plus L-NMMA (71 ± 5 μm) in arterioles. I/R = ischemia/reperfusion; B = before acetylcholine; A = after acetylcholine. *p < 0.05; **p < 0.01.

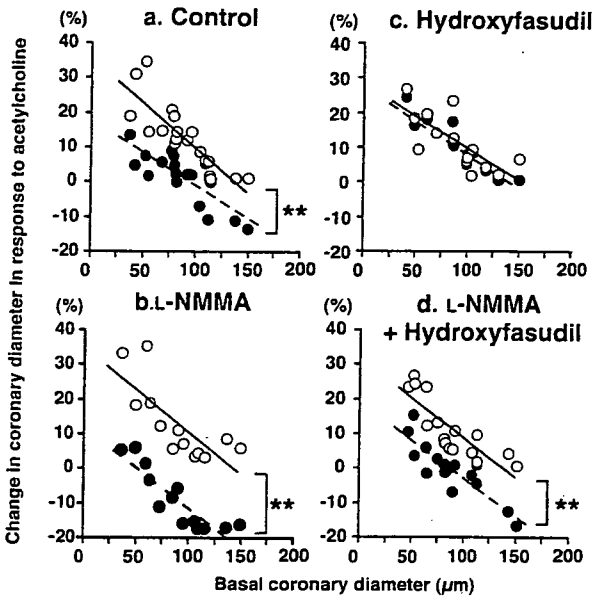


**Figure 5.** Coronary microvascular responses to acetylcholine before and after coronary ischemia/reperfusion (I/R) injury in dogs in vivo. Under control conditions, I/R significantly impaired coronary vasodilator response to acetylcholine (**a**), whereas hydroxyfasudil completely preserved the responses in the absence (**c**) or presence of L-NMMA (**d**) compared with that in the presence of L-NMMA alone (**b**). Number of vessels per animals used was 19/7 under control conditions (before I/R: $y = -0.3x + 35.9$, $r = 0.85$; after I/R: $y = -0.2x + 18.1$, $r = 0.80$), 13/4 for L-NMMA alone (before I/R: $y = -0.2x + 35.1$, $r = 0.76$; after I/R: $y = -0.2x + 12.2$, $r = 0.88$), 14/7 for hydroxyfasudil (before I/R: $y = -0.2x + 27.9$, $r = 0.73$; after I/R: $y = -0.2x + 27.4$, $r = 0.80$), and 16/7 for hydroxyfasudil plus L-NMMA (before I/R: $y = -0.2x + 31.8$, $r = 0.83$; after I/R: $y = -0.2x + 19.2$, $r = 0.86$). **$p < 0.01$. **Open circles** = before I/R; **solid circles** = after I/R.

variables at baseline did not significantly change after I/R compared with those before I/R (Table 1).

**Effects of Rho-kinase inhibition on serotonin-induced coronary responses.** Intracoronary administration of serotonin caused coronary vasoconstriction of small arteries and vasodilation of arterioles under control conditions (Figs. 3a and 3b, both $p < 0.01$ vs. basal coronary diameter). Intracoronary administration of L-NMMA enhanced the serotonin-induced vasoconstriction and abolished the serotonin-induced vasodilation of arterioles (Fig. 3b, $p < 0.01$ vs. serotonin, S). By contrast, hydroxyfasudil reversed the serotonin-induced vasoconstriction of small arteries to vasodilation while it further enhanced the serotonin-induced vasodilation of arterioles (Figs. 3a and 3b, both $p < 0.01$). The vasodilator effect of hydroxyfasudil on the coronary response to serotonin was significantly attenuated by L-NMMA in both-sized arteries (Figs. 3a and 3b, both $p < 0.01$). As a result, serotonin-induced increase in CBF (Fig. 3c) was significantly inhibited by L-NMMA ($p < 0.05$) and enhanced by hydroxyfasudil ($p < 0.05$), the effect of which was significantly attenuated by L-NMMA ($p < 0.01$).

**Endothelium-dependent coronary vasodilation before and after I/R.** Under control conditions (before I/R), intracoronary administration of acetylcholine caused a significant coronary vasodilation to a greater extent in arterioles than in small arteries (Figs. 4a, 4b, and 5a, $p < 0.01$). Coronary I/R significantly impaired the coronary vasodilation to acetylcholine in both sized arteries (both $p < 0.01$) and L-NMMA further reduced the vasodilation (Figs. 4a, 4b, and 5b both $p < 0.01$), whereas hydroxyfasudil completely preserved (small artery $p < 0.05$, arteriole $p < 0.01$) the acetylcholine-induced coronary vasodilator response after I/R (Figs. 4a and 4b). The vasoconstriction by L-NMMA was significantly attenuated by hydroxyfasudil in both sized arteries (both $p < 0.05$) with decrement of CBF (Figs. 4a to 4c). When the coronary vasodilator response to acetylcholine was expressed as a function of basal coronary diameter, hydroxyfasudil preserved the response after I/R injury at all sized coronary arteries either in the absence

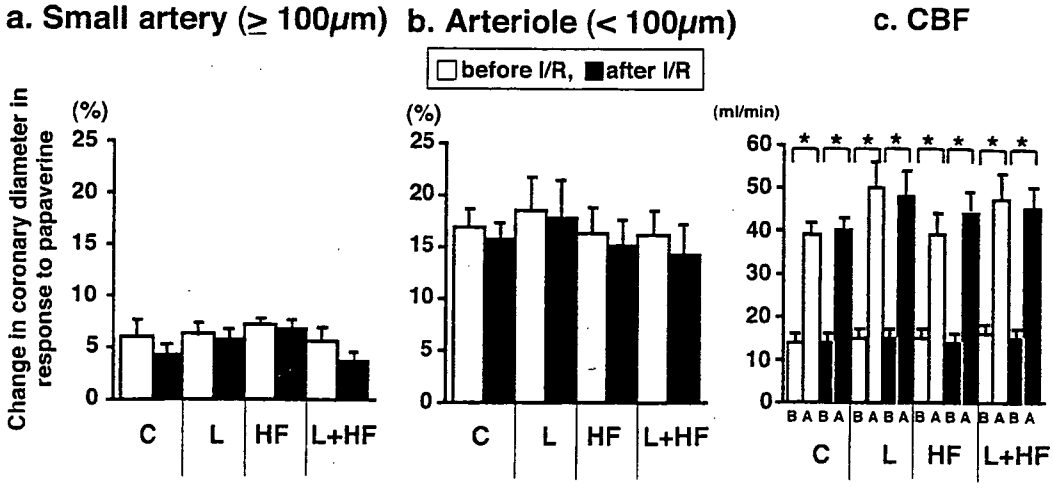


**Figure 6.** Endothelium-independent coronary vasodilation before and after coronary I/R injury in dogs in vivo. Coronary vasodilator response to papaverine was comparable under all conditions in both small arteries and arterioles. Number of vessels per animals used was 7/6 for control (mean diameter 120 ± 7 μm), 5/4 for L-NMMA (123 ± 8 μm), 6/4 for hydroxyfasudil (118 ± 8 μm), and 5/4 for hydroxyfasudil plus L-NMMA (125 ± 9 μm) in small arteries; and 12/6 for control (70 ± 6 μm), 8/4 for L-NMMA (69 ± 7 μm), 8/5 for hydroxyfasudil (68 ± 7 μm), and 11/6 for hydroxyfasudil plus L-NMMA (71 ± 5 μm) in arterioles. C = control; L = L-NMMA; HF = hydroxyfasudil. I/R = ischemia/reperfusion. B = before papaverine; A = after papaverine.

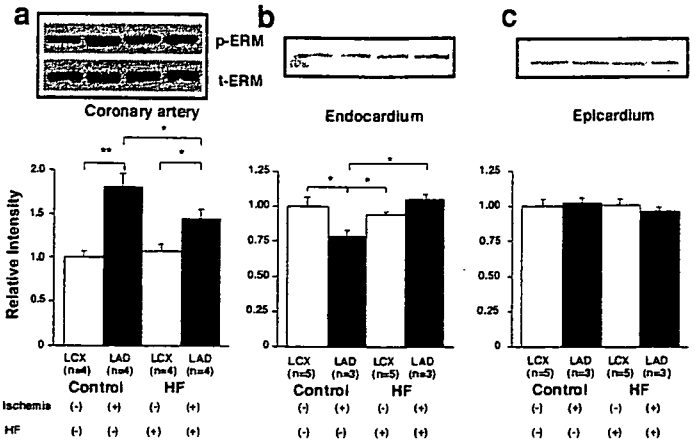


**Figure 7.** Western blotting showing the effects of hydroxyfasudil (HF) on Rho-kinase activity and on eNOS protein expression in the myocardium of LAD and LCX. **(a)** Rho-kinase activity in coronary artery; **(b)** expression of eNOS protein in endocardium; **(c)** expression of eNOS protein in epicardium. Rho-kinase activity was determined by the degree of ezrin-radixin-moesin phosphorylation (p-ERM/t-ERM). Rho-kinase activation in the ischemic LAD was completely inhibited by cotreatment with hydroxyfasudil. Expression of eNOS protein in the ischemic endocardium of LAD area was significantly decreased compared with the non-ischemic endocardium of LCX area, which was again improved by hydroxyfasudil. $^{*}p < 0.05$, $^{**}p < 0.01$.

(Figs. 4a, 4b, and 5c, df 2, 25, $p < 0.01$) or presence (Figs. 4a, 4b, and 5d, df 2, 24, $p < 0.01$) of L-NMMA compared with that in the presence of L-NMMA alone (Figs. 4a, 4b, and 5b).

**Endothelium-independent coronary vasodilation.** Coronary vasodilator response to papaverine was comparable under all conditions in both small arteries and arterioles (Figs. 6a and 6b). Similarly, the increase in CBF to papaverine (Fig. 6c) was also comparable under all conditions in both-sized arteries. Those coronary vasodilator responses were resistant to the blockade of NO synthesis with L-NMMA (Figs. 6a and 6b).

**Activation of Rho-kinase by ischemia-reperfusion causes down-regulation of eNOS protein expression.** Rho-kinase activity after a 90-min period of ischemia was significantly greater in the ischemic LAD than in the nonischemic LCX in the control group (Fig. 7a, $p < 0.01$). This Rho-kinase activation was significantly suppressed by hydroxyfasudil in the ischemic LAD (Fig. 7a, $p < 0.01$). Expression of eNOS protein in the ischemic endocardium of the LAD area (as determined by Western blotting) was significantly decreased (79 ± 4%, $p < 0.05$) compared with the nonischemic endocardium of the LCX area (100 ± 7%), which was also improved by hydroxyfasudil (105 ± 6%) (Fig. 7b, $p < 0.05$). There was no significant difference in the eNOS expression in the epicardium between the LAD and LCX area (Fig. 7c).

**Effect of Rho-kinase inhibition on I/R-induced myocardial infarct size.** Ischemia-reperfusion injury caused myocardial infarct area that was approximately 50% of the left ventricular risk area, and intracoronary L-NMMA did not further increase the I/R-induced infarction size (Fig. 8a). Intracoronary pretreatment with hydroxyfasudil markedly reduced the infarct size ($p < 0.01$ vs. control), and this beneficial effect of hydroxyfasudil was significantly attenuated by L-NMMA (Fig. 8a $p < 0.01$). In the control group, there was an inverse relation between the infarct area and collateral blood flow measured by microsphere technique ($r = 0.93$, $p < 0.01$), and hydroxyfasudil significantly shifted the regression line downward as compared with the control group ($p < 0.01$), that is, smaller infarct size for a given collateral flow (Fig. 8b).

## DISCUSSION

The major findings of the present in vivo study in the canine coronary microcirculation were that: 1) a specific Rho-kinase inhibitor hydroxyfasudil preserved the endothelium-dependent coronary vasodilator responses after coronary I/R injury, 2) hydroxyfasudil also reduced myocardial infarct size, and 3) NO may be involved in those cardiovascular protective effects of hydroxyfasudil. To the best of our knowledge, this is the first report that demonstrates the usefulness of a Rho-kinase inhibitor to prevent coronary I/R injury in vivo.

**Validations of experimental model and methodology.** On the basis of the previous reports (4,12,20), we chose the adequate dose of hydroxyfasudil, acetylcholine, papaverine, and L-NMMA to examine the effects of the Rho-kinase inhibition, endothelium-dependent and -independent vasodilator responses, and inhibition of NO synthesis on coronary vascular responses before and after coronary I/R, respectively. The methodologic validity of the present study has been confirmed previously (15). After 60 to 90 min of ischemia, ultrastructural damage of coronary endothelium was observed particularly in the subendocardium in the present study, a consistent finding to the previous study (21).

**Hydroxyfasudil as a specific Rho-kinase inhibitor in the coronary microcirculation in vivo.** Shimokawa et al. (11) have recently demonstrated that hydroxyfasudil is a specific Rho-kinase inhibitor that markedly inhibits coronary vasospastic responses in a porcine model; its inhibitory effect on Rho-kinase is 100 times greater than on protein kinase C and

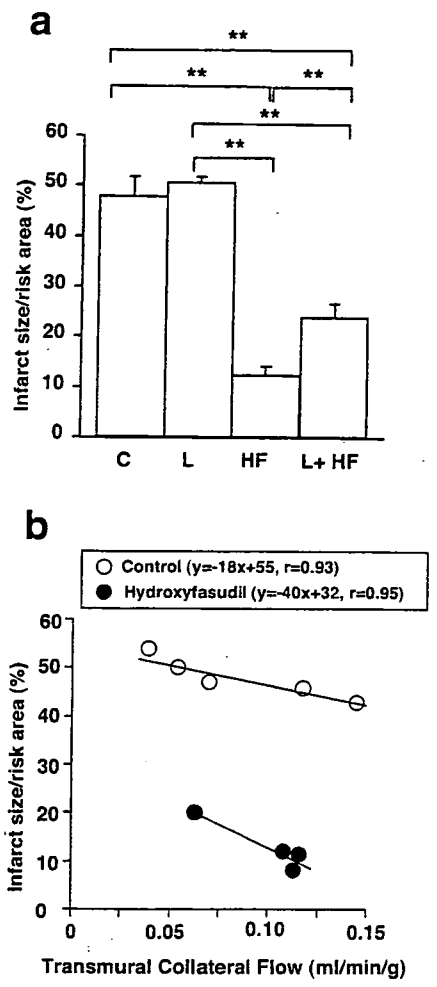


**Figure 8.** (a) Ischemia/reperfusion (I/R)-induced LV infarct size in dogs in vivo. Hydroxyfasudil significantly reduced the I/R-induced LV infarct size. The beneficial effect of hydroxyfasudil was partially attenuated by L-NMMA, while L-NMMA alone did not significantly increase the infarct size. Number of animals used was each 7 for C, HF, and L + HF, and 4 for L. C = control; L = L-NMMA; HF = hydroxyfasudil. **p < 0.01. (b) Plot of infarct size expressed as a percentage of the risk area and regional collateral flow during ischemia. In the control group, there was an inverse relation between infarct area and collateral flow measured by microsphere ($r = 0.93$, $p < 0.01$), and hydroxyfasudil significantly shifted the regression line downward as compared with the control group ($p < 0.01$). Number of animals used was five for control conditions and four for hydroxyfasudil.

1,000 times greater on myosin light-chain kinase. Hydroxyfasudil has potent vasodilator effects on coronary arteries through inhibition of Rho-kinase-mediated phosphorylations of myosin light chains (11). In the present study, intracoronary hydroxyfasudil caused coronary microvascular vasodilation in a dose-dependent manner in vivo, and its vasodilator effect was greater in arterioles than in small arteries (Fig. 2). Hydroxyfasudil suppressed the serotonin-induced vasoconstriction of small arteries, whereas it enhanced the serotonin-induced vasodilation of arterioles in vivo (Fig. 3). This finding is in accordance with the hypothesis that the calcium sensitization of vascular smooth-muscle cells mediated by Rho-kinase plays a key role in the molecular mechanisms of coronary hyperconstriction (12). Furthermore, in the present study, intracoronary L-NMMA significantly attenuated serotonin-induced coronary vasodilator responses, which were improved by hydroxyfasudil, indicating an involvement of NO-mediated mechanism in the beneficial effects of the Rho-kinase inhibitor. Lamping et al. (22) demonstrated that coronary vascular response to serotonin is determined by a balance between 5-$HT_1$ receptor-mediated dilatation of coronary arterioles and 5-$HT_2$ receptor-mediated vasoconstriction of small coronary arteries. Inhibition of NO synthase enhances coronary vasoconstriction to serotonin in both-sized arteries. Our present results are in agreement with those of Lamping et al. The beneficial vasodilator effect of hydroxyfasudil on coronary vascular response to serotonin is mediated by its action on both vascular smooth muscle and the endothelium as shown in Figure 3. Thus, it is possible that the beneficial effect of Rho-kinase blockade with hydroxyfasudil is mediated by its action on both vascular smooth muscle and the endothelium (22). Serotonin released by aggregating platelets has been implicated for coronary vasospasm in the presence of damaged vascular endothelium (5,23).

**Beneficial effects of a Rho-kinase inhibitor on coronary I/R injury.** In the present study, hydroxyfasudil exerted beneficial effects on I/R-induced endothelial injury in the canine coronary microcirculation in vivo through the NO-dependent mechanism (Figs. 4 and 5). This dose of hydroxyfasudil (100 μg/kg) selectively inhibits Rho-kinase activity and effectively prevents serotonin-induced coronary hyperconstriction. Recent studies have demonstrated that cGMP-dependent protein kinase inhibits RhoA phosphorylation by inhibiting the membrane binding of RhoA, in which the NO-mediated mechanism may inhibit the RhoA/Rho-kinase pathway (24–26). It was previously demonstrated that statins attenuate I/R injury of the heart and the brain in rats and mice, demonstrating the Rho-mediated and NO-dependent protective effect of statins (27,28). Hydroxyfasudil also inhibits the production of superoxide anions in neutrophils (29) and various chemoattractant-induced migration of those cells (14) in a canine model of cerebral ischemia. Furthermore, treatment with hydroxyfasudil in human saphenous vein endothelial cells reversed the hypoxia-induced decrease in eNOS activity as examined by the citrulline conversion assay and 4,5-diaminofluorescein diacetate fluorescence method (13). In the present study, I/R increased Rho-kinase activity, and hydroxyfasudil significantly inhibited the Rho-kinase activation. These findings suggest that NO is involved in the protective effect of hydroxyfasudil with an increase in eNOS activity and a decrease in Rho-kinase activity during reperfusion injury.

In the present study, the vasodilator effects of hydroxyfasudil were significantly attenuated by L-NMMA (Figs. 3 and 4). The eNOS expression was decreased in the ischemic area of the endocardium compared with that of the epicardium under control conditions, which was improved by hydroxyfasudil (Fig. 7). We have previously demonstrated that endocardial arteriolar dilation during reactive hyperemia is more sensitive to L-NMMA than epicardial arte-

JACC Vol. 45, No. 4, 2005
February 15, 2005:599–607

**Table 1.** Hemodynamics During Myocardial Ischemia-Reperfusion Injury in Dogs

| | n | Before I/R | | | After I/R | | |
|---|---|---|---|---|---|---|---|
| | | Baseline | ACh | Papaverine | Baseline | ACh | Papaverine |
| MBP (mm Hg) | | | | | | | |
| Control | 7 | 91 ± 4 | 90 ± 6 | 92 ± 5 | 89 ± 4 | 89 ± 5 | 92 ± 6 |
| L-NMMA | 4 | 88 ± 8 | 86 ± 5 | 91 ± 7 | 86 ± 4 | 86 ± 4 | 85 ± 4 |
| Hydroxyfasudil | 7 | 92 ± 9 | 92 ± 8 | 93 ± 8 | 93 ± 6 | 90 ± 6 | 91 ± 7 |
| L-NMMA + hydroxyfasudil | 7 | 89 ± 6 | 89 ± 5 | 89 ± 5 | 91 ± 8 | 87 ± 10 | 89 ± 9 |
| Heart rate (beats/min) | | | | | | | |
| Control | 7 | 151 ± 5 | 156 ± 3 | 155 ± 3 | 155 ± 5 | 153 ± 5 | 152 ± 5 |
| L-NMMA | 4 | 147 ± 7 | 149 ± 8 | 149 ± 8 | 145 ± 11 | 146 ± 11 | 145 ± 11 |
| Hydroxyfasudil | 7 | 152 ± 7 | 151 ± 8 | 148 ± 8 | 148 ± 7 | 149 ± 7 | 150 ± 7 |
| L-NMMA + hydroxyfasudil | 7 | 151 ± 6 | 152 ± 6 | 151 ± 6 | 154 ± 6 | 151 ± 6 | 153 ± 7 |

Results are expressed as mean ± SEM.
ACh = acetylcholine; I/R = ischemia/reperfusion; MBP = mean blood pressure.

riolar dilation (30). These findings indicate that the perfusion of the endocardium is more dependent on NO than that of the epicardium and that endothelial damage after I/R in arterioles may be greater in the endocardium than in the epicardium.

In the present study, hydroxyfasudil exerted cardiovascular protective effects on coronary I/R injury, as did preconditioning (31,32). However, the mechanism by which hydroxyfasudil and preconditioning protect coronary I/R injury appears to be different. Endogenous NO does not alter the infarct size after I/R and is not involved in the protective mechanism of preconditioning in pigs or rabbits (33,34). It has been suggested that preconditioning preserves myocardial creatine phosphate and intracellular pH (35). Furthermore, ischemic preconditioning increases adenosine production and activates protein kinase C, which also enhances adenosine production during I/R injury.

In the present study, hydroxyfasudil significantly reduced myocardial infarct size with increment of coronary collateral blood flow, at least in part, thorough the NO-mediated mechanism (Fig. 8). Shimokawa et al. (11) demonstrated that hydroxyfasudil inhibits both MLC mono- and diphosphorylations. Satoh et al. (14) showed that hydroxyfasudil also protects the brain from ischemic injury through inhibition of superoxide production and neutrophil infiltration. Mohri et al. (36) demonstrated that fasudil suppresses coronary microvascular spasm in patients with microvascular angina. Wolfrum et al. (37) recently demonstrated that inhibiting Rho-kinase has cardioprotective effects to reduce infarct size by activating phosphatidylinositol 3-kinase/protein kinase Akt/eNOS pathways. All these mechanisms may be involved in the beneficial effects of hydroxyfasudil on the I/R-induced myocardial injury.

Hydroxyfasudil increases blood supply to the ischemic region of the myocardium and prevents I/R-induced myocardial injury. Furthermore, it has been recently demonstrated that an estrogen receptor modulator, raloxifene, also reduces I/R-induced myocardial infarct size, whereas an inhibitor of NO synthesis (L-NAME) or a blocker of calcium-activated $K^+$ channels (charybdotoxin) partly attenuates the effect of raloxifene (19). These results suggest that cardioprotective effects of those inhibitors may be mediated in part by the compensatory effects of NO and endothelium-derived hyperpolarizing factor (20). Several studies using NO synthase inhibitors (38,39) or eNOS-deficient mice (40) demonstrated an increase in infarct size after I/R. The effect of NO synthesis inhibition on the infarct size might be species- and dose-dependent.

**Clinical implications and conclusions.** The present study has demonstrated for the first time that hydroxyfasudil, a specific Rho-kinase inhibitor, has NO-dependent cardiovascular protective effects on coronary I/R injury in vivo. Rho-kinase inhibitor has also an antianginal effect in a canine model of angina (41), patients with effort angina (42), and those with vasospastic angina (43). Moreover, it has been recently reported that hydroxyfasudil may be effective for the treatment of pulmonary hypertension (44). Indeed, Rho-kinase inhibitors may be useful for the treatment of a wide range of cardiovascular diseases (10). The present study suggests that Rho-kinase inhibitors may also be useful for the treatment of coronary I/R injury in humans.

## Acknowledgment

We thank Y. Matsuo for excellent technical assistance in this study.

**Reprint requests and correspondence:** Dr. Toyotaka Yada, Kawasaki Medical School, 577 Matsushima, Kurashiki, Okayama, 701-0192, Japan. E-mail: yada@me.kawasaki-m.ac.jp.

## REFERENCES

1. Vanbenthuysen PJ, McMurtry IF, Horwitz LD, et al. Reperfusion after acute coronary occlusion in dogs impairs endothelium-dependent relaxation to acetylcholine and augments contractile reactivity in vitro. J Clin Invest 1987;79:265–74.
2. Pearson PJ, Schaff HV, Vanhoutte PM, et al. Acute impairment of endothelium-dependent relaxations to aggregating platelets following reperfusion injury in canine coronary arteries. Circ Res 1990; 67:385–93.
3. Mehta JL, Nichols WW, Donnelly WH, et al. Impaired canine coronary vasodilator response to acetylcholine and bradykinin after occlusion-reperfusion. Circ Res 1989;64:43–54.

4. Defily DV, Chilian WM. Preconditioning protects coronary arteriolar endothelium from ischemia-reperfusion injury. Am J Physiol 1993; 265:H700-6.
5. Vanhoutte PM, Shimokawa H. Endothelium-derived relaxing factor and coronary spasm. Circulation 1989;80:1-9.
6. Korthuis RJ, Granger DN, Townsley MI, et al. The role of oxygen-derived free radicals in ischemia-induced increases in canine skeletal muscle vascular permeability. Circ Res 1985;57:599-609.
7. Olafsson B, Forman MB, Puett DW, et al. Reduction of reperfusion injury in the canine preparation by intracoronary adenosine: importance of the endothelium and the no-reflow phenomenon. Circulation 1987;76:1135-45.
8. Lamping KG, Marcus ML, Dole WP. Removal of endothelium potentiates canine large coronary artery constrictor response to 5-hydroxytryptamine in vivo. Circ Res 1985;57:46-54.
9. Cohen RA, Shepherd JT, Vanhoutte PM. 5-hydroxytryptamine can mediate endothelium-dependent relaxation of coronary arteries. Am J Physiol 1983;245:H1077-80.
10. Shimokawa H. Rho-kinase as a novel therapeutic target in treatment of cardiovascular diseases. J Cardiovasc Pharmacol 2002;39:319-27.
11. Shimokawa H, Seto M, Katsumata N, et al. Rho-kinase-mediated pathway induces enhanced myosin light chain phosphorylations in a swine model of coronary artery spasm. Cardiovasc Res 1999;43: 1029-39.
12. Kandabashi T, Shimokawa H, Miyata K, et al. Inhibition of myosin phosphatase by upregulated Rho-kinase plays a key role for coronary artery spasm in a porcine model with interleukin-1$\beta$. Circulation 2000;101:1319-23.
13. Takemoto M, Sun J, Hiroki J, et al. Rho-kinase mediates hypoxia-induced downregulation of endothelial nitric oxide synthase. Circulation 2002;106:57-62.
14. Satoh S, Utsunomiya T, Tsurui K, et al. Pharmacological profile of hydroxy fasudil as a selective Rho-kinase inhibitor on ischemic brain damage. Life Sci 2001;69:1441-53.
15. Yada T, Hiramatsu O, Kimura A, et al. In vivo observation of subendocardial microvessels of the beating porcine heart using a needle-probe videomicroscope with a CCD camera. Circ Res 1993; 72:939-46.
16. Mori HS, Haruyama Y, Shinozaki H, et al. New nonradioactive microspheres and more sensitive X-ray fluorescence to measure regional blood flow. Am J Physiol 1992;263:H1946-57.
17. Laufs U, Fata VL, Liao JK. Inhibition of 3-hydroxy-3-methylglutaryl (HMG)-CoA reductase blocks hypoxia-mediated down-regulation of endothelial nitric oxide synthase. J Biol Chem 1997;272:31725-9.
18. Katsura M, Mohri Y, Shuto K, et al. Up-regulation of L-type voltage-dependent calcium channels after long term exposure to nicotine in cerebral cortical neurons. J Biol Chem 2002;277:7979-88.
19. Ogita H, Node K, Asanuma H, et al. Amelioration of ischemia- and reperfusion-induced myocardial injury by the selective estrogen receptor modulator, raloxifene, in the canine heart. J Am Coll Cardiol 2002;40:998-1005.
20. Yada T, Shimokawa H, Hiramatsu O, et al. Hydrogen peroxide, an endogenous EDHF, plays an important role in coronary autoregulation in vivo. Circulation 2003;107:1040-5.
21. Ehring T, Krajcar M, Baumgart D, et al. Cholinergic and $\alpha$-adrenergic coronary constriction with increasing ischemia-reperfusion injury. Am J Physiol 1995;268:H886-94.
22. Lamping KG. Enhanced contractile mechanisms in vasospasm: is endothelial dysfunction the whole story? Circulation 2002;105: 1520-2.
23. Golino P, Ashton JH, Buja LM, et al. Local platelet activation causes vasoconstriction of large epicardial canine arteries in vivo: thromboxane A2 and serotonin are possible mediators. Circulation 1989;79: 154-66.
24. Chitaley K, Webb RC. Nitric oxide induces dilation of rat aorta via inhibition of Rho-kinase signaling. Hypertension 2002;39:438-42.
25. Sauzeau V, Le Jeune H, Cario-Toumaniantz C. Cyclic GMP-dependent protein kinase signaling pathway inhibits RhoA-induced $Ca^{++}$ sensitization of contraction in vascular smooth muscle. Biol Chem 2000;275:21722-9.
26. Sawada N, Itoh H, Yamashita J, et al. Cyclic GMP-dependent protein kinase phosphorylates and inactivates RhoA. Biochem Biophys Res Commun 2001;280:798-805.
27. Ikeda Y, Lindon HY, Lefer AM. Rosuvastatin, a new HMG-CoA reductase inhibitor, protects ischemic reperfused myocardium in normocholesterolemic rats. J Cardiovasc Pharmacol 2003;41:649-56.
28. Amin-Hanjani S, Stagliano NE, Yamada M, et al. Mevastatin, an HMG-CoA reductase inhibitor, reduces stroke damage and upregulates endothelial nitric oxide synthase in mice. Stroke 2001;32:980-6.
29. Arai M, Sasaki Y, Nozawa R. Inhibition by the protein kinase inhibitor HA1077 of the activation of NADPH oxidase in human neutrophils. Biochem Pharmacol 1993;46:1487-90.
30. Yada T, Hiramatsu O, Kimura A, et al. Direct in vivo observation of subendocardial arteriolar responses during reactive hyperemia. Circ Res 1995;77:622-31.
31. Murry CE, Jennings RB, Reimer KA. Preconditioning with ischemia: a delay of lethal cell injury in ischemic myocardium. Circulation 1986;74:1124-36.
32. Cohen MV, Liu GS, Downey JM. Preconditioning causes improved wall motion as well as smaller infarcts after transient coronary occlusion in rabbits. Circulation 1991;84:341-9.
33. Post H, Schulz R, Behrends M, et al. No involvement of endogenous nitric oxide in classical ischemic preconditioning in swine. J Mol Cell Cardiol 2000;32:725-33.
34. Nakano A, Liu GS, Heusch G. Exogenous nitric oxide can trigger a preconditioning state through a free radical mechanism, but endogenous nitric oxide is not a trigger of classical ischemic preconditioning. J Mol Cell Cardiol 2000;32:1159-67.
35. Kida M, Fujiwara H, Ishida M, et al. Ischemic preconditioning preserves creatine phosphate and intracellular pH. Circulation 1991; 84:2495-503.
36. Mohri M, Shimokawa H, Hirakawa Y, et al. Rho-kinase inhibition with intracoronary fasudil prevents myocardial ischemia in patients with coronary microvascular spasm. J Am Coll Cardiol 2003;41:15-9.
37. Wolfrum S, Dendorfer A, Rikitake Y, et al. Inhibition of rho-kinase leads to rapid activation of phosphatidylinositol 3-kinase/protein kinase akt and cardiovascular protection. Arterioscler Thromb Vasc Biol 2004;24:1-6.
38. Williams MW, Taft CS, Ramnauth S, et al. Endogenous nitric oxide (NO) protects against ischaemia-reperfusion injury in the rabbit. Cardiovasc Res 1995;30:79-86.
39. Hoshida S, Yamashita N, Igarashi J, et al. Nitric oxide synthase protects the heart against ischemia-reperfusion injury in rabbits. J Pharmacol Exp Ther 1995;274:413-8.
40. Jones SP, Girod WG, Palazzo AJ, et al. Myocardial ischemia-reperfusion injury is exacerbated in absence of endothelial cell nitric oxide synthase. Am J Physiol 1999;276:H1567-73.
41. Utsunomiya T, Satoh S, Ikegaki I, et al. Antianginal effects of hydroxyfasudil, a Rho-kinase inhibitor, in a canine model of effort angina. Br J Pharmacol 2001;134:1724-30.
42. Shimokawa H, Hiramori K, Iinuma H, et al. Anti-anginal effect of fasudil, a Rho-kinase inhibitor, in patients with stable effort angina: a multicenter study. J Cardiovasc Pharmacol 2002;40:751-61.
43. Masumoto A, Mohri M, Shimokawa H, et al. Suppression of coronary artery spasm by the Rho-kinase inhibitor fasudil in patients with vasospastic angina. Circulation 2002;105:1545-7.
44. Abe K, Shimokawa H, Morikawa K, et al. Long-term treatment with a Rho-kinase inhibitor improves monocrotaline-induced fatal pulmonary hypertension in rats. Circ Res 2004;94:385-93.

# Flow-Independent Myocardial Ischemia Induced by Endothelin-1

## An NADH Fluorescence Analysis

*Soushin Inoue, MD,* Shingo Hori, MD,† Takeshi Adachi, MD,‡ Koji Miyazaki, MD,* Shingo Kyotani, MD,§ Keiichi Fukuda, MD,* Hidezo Mori, MD,§ Hiroe Nakazawa, MD,¶ Naoki Aikawa, MD,† and Satoshi Ogawa, MD**

**Abstract:** The endothelin-1 (ET-1) is known to cause myocardial ischemia; however, whether this effect is entirely dependent on vasoconstriction is uncertain. The aim of this study was to characterize the myocardial ischemia after the intracoronary administration of endothelin-1, and compare it with that induced by coronary stenosis. In the left anterior descending coronary artery of 15 dogs, a mild inflow reduction (30%) was produced for 10 minutes using intracoronary endothelin-1 (46 ± 33 pmol/min) or coronary stenosis. The hearts were rapidly cross-sectioned at short axial plane and freeze-clamped within 120 milliseconds using a specially developed device to visualize and quantify the area of ischemia (%IA) with NADH fluorescence photography. The %IA was larger in the endothelin-1 group than in the stenosis group (66 ± 23 versus 18 ± 18, $P = 0.0005$); furthermore, the ischemia was transmural in the ET-1 group, but limited to subendocardium in the stenosis group. ET-1 increased the coronary arterial resistance especially in subepicardial region and produced smaller ischemic foci in microcirculation. The mechanism of larger ischemia produced by ET-1 might depend on pro-ischemic effects on myocytes and vasoconstriction of the coronary microcirculation, predominantly in the subepicardium in vivo.

**Key Words:** coronary circulation, endothelin-1, microcirculation, myocardial ischemia, NADH fluorescence, pro-ischemia

(*J Cardiovasc Pharmacol*™ 2005;46:810–816)

Endothelin-1 (ET-1) is the most potent vasoactive peptide derived from the endothelium[1] and constricts vascular smooth muscles to induce hypoperfusion.[2] The plasma ET-1 was found to be increased in patients with acute myocardial infarction and angina pectoris.[3] The pathophysiological role of ET-1 for ischemic heart disease is relevant but not fully clarified yet. Others and we have previously reported that the intracoronary administration of ET-1 induces a prominent coronary flow reduction, ST elevation, apical systolic bulge, and impaired left ventricular diastolic function in vivo.[4–6] The reduced cardiac function with ST-elevation indicated that ET-1 induces myocardial ischemia by decreasing coronary flow. However, the systolic bulge induced by ET-1 was unexpected and could not be explained by standard criteria for myocardial ischemia using a reduced flow model, which predominantly decreases the subendocardial blood flow.[4] Moreover, ET-1 receptor antagonists were shown to reduce the myocardial infarction size in ischemia/reperfusion models without any changes in regional myocardial blood flow, suggesting that intrinsic ET-1 has a flow-independent effect on myocardial ischemia in vivo.[7,8] In addition to its vasoconstrictive effect, ET-1 has direct effects on cardiac myocytes, including positive inotropic, chronotropic, and metabolic effects.[9–12] Therefore, myocardial ischemic metabolism and flow distribution should be compared in ET-1 administration and simple flow-reduction models.

The aim of this study was to clarify the characteristics of myocardial ischemia induced by the intracoronary administration of ET-1 under condition of controlled mild hypoperfusion in a canine model. The extension, distribution, and severity of myocardial ischemia induced by ET-1 were compared with those induced by an equivalent coronary flow reduction introduced by occluding the bypass circuit to the coronary artery. Because the severity and the distribution of metabolic changes in ET-1–induced myocardial ischemia were not quantified in previous reports, the flow-dependent and -independent pro-ischemic effects of ET-1 have not been sufficiently differentiated. In this study, we applied an NADH fluorescence method to rapidly cross-sectioned frozen heart slices, because NADH is a sensitive marker of ischemia and the distribution of the myocardial ischemic region can be clearly visualized by UV fluorescence. Regional metabolite sampling from frozen heart tissue also reveals the distribution and severity of ischemic myocardium.[13,14] This specially developed sampling method has been shown to be rapid enough to preserve the redox states that existed prior to sectioning, because the sectioning and freezing is performed within 120 milliseconds.[13]

Received for publication April 29, 2005; accepted September 12, 2005.

From the *Cardiopulmonary Division, Department of Internal Medicine, Keio University School of Medicine, Tokyo, Japan; †Department of Emergency and Critical Care Medicine, Keio University School of Medicine, Tokyo, Japan; ‡Department of Biochemistry and Integrative Medical Biology, Keio University School of Medicine, Tokyo, Japan; §National Cardiovascular Center; and ¶Department of Physiology, Tokai University School of Medicine.

Reprints: Shingo Hori, Department of Emergency Medicine, Keio University School of Medicine, 35 Shinanomachi, Shinjuku-ku, Tokyo, 160-8582 Japan (e-mail: shingo@sc.itc.keio.ac.jp).

## METHODS

The present investigation conformed with the guidelines for the care and use of laboratory animals published by the US National Institutes of Health (NIH publication No. 85-23, revised 1985).

### Animal Preparation

Mongrel dogs weighing 9 to 12 kg (n = 22) were anesthetized with pentobarbital (35 mg/kg iv) and sustained under positive-pressure ventilation. A bilateral thoracotomy was performed at the sixth intercostal space, and the heart was suspended in a pericardial cradle. Heparin was administered intravenously at 500 units/kg. To measure the aortic pressure, a 7F catheter was introduced from the femoral artery into the ascending aorta. A bypass made of silicon tube with metal tip was cannulated from a left subclavian artery to the left anterior descending coronary artery (LAD) on beating heart. The proximal LAD was ligated and cut down to insert a metal tip of the bypass. The diameter of left subclavian artery may not be suitable for coronary diameter but is applicable for bypass-supplier because of avoiding operative failure and excessive bleeding on preparation. A pressure transducer (TP400P, Nihon Koden, Co. Ltd., Tokyo, Japan) and an electromagnetic flow probe (MFV-1200, Nihon Koden, Co. Ltd.) were installed on the bypass circuit, and the coronary perfusion pressure and coronary blood flow were continuously monitored and recorded at thermograph. To record the epicardial electrocardiogram, an electrode made of Ag-AgCl was placed at the center of the perfused area of the left anterior descending coronary artery. To administer the fluorescent dye or non-radioactive microspheres, a 7F catheter was inserted into the left cardiac auricle. The heart rate was fixed at 200 beats per min (bpm) using left atrial pacing. Before starting the experimental protocol, the bypass circuit was occluded for 15 seconds and dogs with reactive hyperemia below 200% of the control flow level were excluded from the study.

### Protocol 1: Visualization of Tissue Redox State and Chemical Analysis of Myocardial Ischemia

Fifteen dogs were randomly divided into two groups; eight received the ET-1 administration (endothelin group) and seven underwent coronary stenosis (stenosis group). In the endothelin group, ET-1 (Peptide Institute Inc., Osaka, Japan; 10–150 pmol/min) was administered continuously into the silicon bypass circuit using a micro-infusion pump[15]: this dose reduced the coronary flow by 20% to 40% of the control level. The dosage of ET-1 rapidly increased within 1 minute to get the target flow reduction. The same speed of ET-1 injection could keep in steady state flow reduction, but some dogs with reduced flow level over 40% were excluded from the study. In the stenosis group, coronary inflow was reduced to a comparable level (20%–40% of the control level) by mechanical constriction of the bypass tube. The hemodynamic parameters and epicardial electrocardiogram (ECG) were recorded every minute. The ST segment of the epicardial ECG was measured at 100 milliseconds from the initiation of the QRS complex. At 10 minutes after coronary flow reduction, the beating heart was rapidly cross-sectioned into 4-mm-thick slices along the short-axis plane of the left ventricle using a sampling device specially developed by Hori et al.[13] Within 120 milliseconds after cross-sectioning, a cross-sectional heart slice was compressed to 2.4-mm thickness using precooled aluminum blocks at −190°C. To visualize the tissue redox state of the bypass-perfused areas, from where the cross-sectioned heart slices were obtained, 10 mL of fluorescent dye solution (rhodamine B fluid: 0.1 mg/mL/kg) was injected into the left cardiac auricle 5 seconds before cross-sectioning. The frozen heart slices were fixed in a specially made container filled with precooled freon-12 ($CCl_2F_2$) and preserved in liquid nitrogen.

### Visualization of Tissue Redox State by NADH Fluorescence Imaging

The increase in NADH is the most sensitive and rapid intracellular reaction to occur during ischemia[16,17] and can be visualized as an increase in the NADH fluorescence level in ischemic myocardium. Dual fluorescence photography of NADH (indicating ischemia) and rhodamine B (indicating bypass non-perfused areas) was applied to 15 frozen heart slices. A pair of excitation lights (360 nm, Model B-100A, Ultra-Violet Products, CA) was applied to the frozen heart slices at liquid-nitrogen temperature to visualize the surface NADH and rhodamine B fluorescence in the cross-sectional plane. Two band pass filters were used as secondary filters (Kodak Wratten Gelatin Filter 2E and 47 (Kodak Japan Co. Ltd., Tokyo, Japan) for NADH fluorescence, Kenko Optical Filter YA-3 (Kenko Co. Ltd, Tokyo, Japan) for rhodamine B fluorescence). To quantify the area of myocardial ischemia, the surface NADH fluorescence was analyzed using an image analyzer (IBAS, Carl Zeiss Japan Co. Ltd., Tokyo, Japan) via a CCD video camera (XC-77, Sony Japan Co. Ltd., Tokyo, Japan). A positive NADH-fluorescent area (ischemic area) was defined as an area with a fluorescence intensity two standard deviations above the mean of the simultaneously measured control frozen slice, given another non-ischemic canine cross-sectional heart sample. The bypass-perfused area was defined as the rhodamine B fluorescence-negative area. In a previous study, we observed that rhodamine B, injected into the left cardiac auricle before 5 minutes of cross-sectioning, was not identified in bypass-perfused areas and was clearly present in non-perfused areas.[14] To quantify the amount of ischemic myocardium in the heart slices, the extent of ischemia was expressed as a percentage of the NADH-fluorescent area to the bypass-perfused area in the subendocardial and subepicardial halves of the frozen slices.

To visualize the fluorescent area at a high resolution of up to 10 micrometers, magnified NADH fluorescence photography (×100) was also applied using a dissecting microscope and a Xenon excitation light (Supercure-201S, Fibernics Co. Ltd., Saitama, Japan). To measure the area of microischemia, ischemic foci at the microcirculatory level were selected at random in the endothelin group (1191 counts from 8 randomly selected hearts) and the stenosis group (703 counts from 7 randomly selected hearts). An image analyzer (IBAS, Carl Zeiss Japan Co. Ltd.) was used to measure their short-axis diameters.

### Chemical Analysis for Myocardial Metabolites

Cylindrical microsamples weighing about 10 mg (2.4 mm in diameter and 2.4 mm in depth) were drilled in the liquid-nitrogen frozen slices; the microsamples were obtained in perfused area of the subendocardium or subepicardium exhibiting NADH fluorescence. NADH fluorescence was used as a guide to select the sampling sites. Four to six microsamples from each heart slice, for a total of 62 microsamples, were obtained. The NAD, NADH, ATP, creatine phosphate (CP), and lactate concentrations were analyzed in each microsample. NAD and NADH were measured using the bacterial luciferase method,[18] ATP and creatine phosphate were measured using the luciferin-luciferase method,[13] and lactate was measured using the LDH method.[19] The protein content was determined using the Lowry method.[20]

## Protocol 2: Systemic and Coronary Hemodynamics

To measure myocardial tissue flow without affecting myocardial ischemia in the same animal, coronary flow was successively reduced in an additional seven dogs, first by stenosis and then by ET-1. After performing a baseline measurement (control group), the bypass was constricted and tissue flow was measured after 10 minutes (stenosis group). The stenosis was then released and once the hyperemia had stabilized, ET-1 (10–150 pmol/min) was administered intracoronary to induce the same degree of hypoperfusion and tissue flow was measured again after 10 minutes (endothelin group). Because of the sustained vasoconstriction induced by ET-1, the order of hypoperfusion induced was fixed, not random.

Myocardial tissue flow was measured using nonradioactive microspheres (15 micrometers in diameter), made of inert plastic labeled with stable heavy elements (Sekisui Plastic Co. Ltd., Tokyo, Japan).[21] Microspheres labeled with barium, iodide, zirconium, or bromine were suspended in 0.1% sodium dodecyl sulfate (SDS) solution, and $0.5–1.0 \times 10^7$ microspheres were infused into the left cardiac auricle. The microspheres were well shaken, and mixed mechanically in a syringe prior to or during the protocol, and no aggregations were observed using light microscopy. Heart tissue samples weighing 3 to 5 g were taken from the subendocardial and subepicardial layers of the bypass-perfused area. Tissues and reference arterial blood samples were dissolved in 1N-KOH, and the microspheres were trapped on filter papers. The samples were irradiated with X-rays, and the X-ray fluorescence activity of each heavy element was measured, the amount of microspheres and the tissue flow in each sample were then calculated.

## Statistical Analysis

All values were presented as the means ± SD. Changes in tissue flow and hemodynamic data were determined using a two-way ANOVA. For paired or unpaired data between two groups, Student *t* test was used. *P* values of less than 0.05 were considered statistically significant.

# RESULTS

## Protocol 1

### Hemodynamics and Epicardial Echocardiography

The mean aortic pressures before the experimental protocol were not significantly different between the endothelin group and the stenosis group (Table 1). The hemodynamics did not change significantly throughout the experimental period. The mean doses of endothelin-1 were 46 ± 33 pmol/min. No significant difference in coronary flow reduction was seen in either the endothelin group or the stenosis group. In contrast, the changes in the epicardial ST segment were significantly larger in the endothelin group than in the stenosis group. These results suggest that the myocardial ischemia caused by endothelin-1 differed from that caused by coronary stenosis.

### Extension and Distribution of NADH Fluorescence

Figure 1 shows NADH fluorescence photographs of frozen heart slices from both groups. Myocardial ischemia was transmurally distributed in the endothelin group, whereas ischemia distribution was limited to the subendocardium in the stenosis group. Consequently, the total area of myocardial ischemia was larger in the endothelin group than in the stenosis group (Table 2).

Magnified fluorescence photography (×100) was applied to evaluate ischemia formation at the microcirculatory level. Microischemic spots, round or rectangular in shape depending on the direction of the myocardial fibers, were observed in both groups (Fig. 2, upper photographs). To measure the size of the ischemic spots, the short-axis length of the spot was calculated (Fig. 2, lower bar graph). The mean value of the short-axis diameter (less than 120 micrometers) was significantly smaller in the endothelin group than in the stenosis group (61.1 ± 18 versus 76.4 ± 18 micrometers; $P < 0.0001$).

TABLE 1. Changes in ST Segment and Hemodynamics

| | Endothelin Group (n = 8) Mean (SD) | Stenosis Group (n = 7) Mean (SD) | Statistics |
|---|---|---|---|
| Changes in ST segment (mV) | 6.5 (4.5) | 0.7 (0.5) | $P = 0.006$ |
| Coronary blood flow reduction (%) | 32.3 (4.5) | 34.0 (4.2) | ns |
| Heart rate (/min) | 186 (20) | 200 (3.3) | ns |
| Mean aortic pressure (mm Hg) | 99 (8.7) | 109 (12) | ns |
| Mean coronary perfusion pressure (mm Hg) | 99 (8.3) | 64 (12) | $P < 0.0001$ |

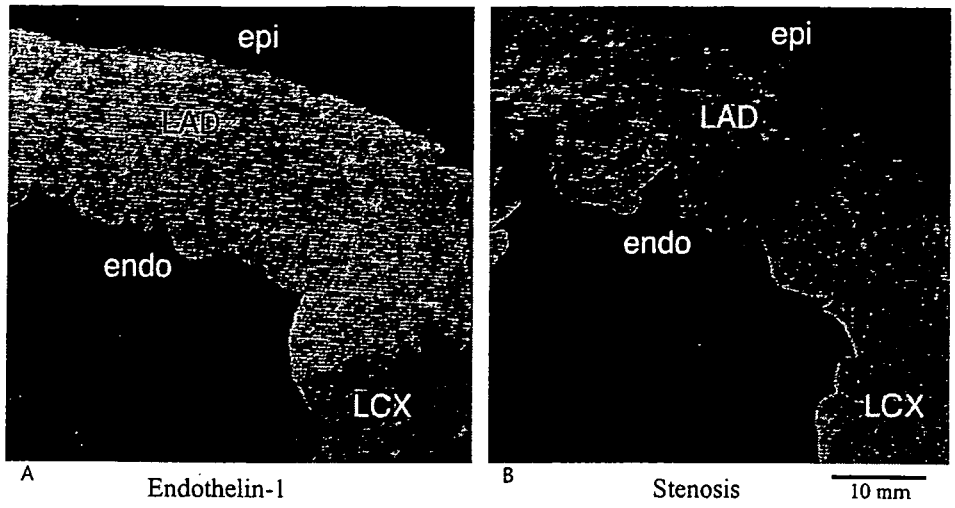


FIGURE 1. NADH fluorescence photographs of cross-sectional frozen heart slices. The slices show short-axial view at mid-left ventricle. LAD, left anterior descending coronary artery perfused myocardium; LCX, left circumflex coronary artery perfused myocardium; Epi, Epicardial side; Endo, Endocardial side. A, Endothelin-1 decreased coronary inflow by 36% and produced a transmural extension of positive NADH fluorescence. B, Stenosis reduced coronary inflow by 32% and produced positive NADH fluorescence (ischemia) in the subendocardium.

### Chemical Analyses of Tissue Metabolites

The higher NADH content as well as the lower NAD/NADH ratio in both the subepicardial and the subendocardial layers of the ischemic LAD areas in the endothelin group indicated more severe anaerobic metabolism than in the stenosis group (Table 3). These indicators are the most sensitive marker of the redox states in ischemic myocardium; no difference in classic ischemic markers like lactate, ATP, or CP were observed between the two treatment groups (Table 3).

In NADH-fluorescent myocardium, the NADH concentrations were significantly higher than those in NADH-non–fluorescent areas (0.77 ± 0.20 versus 0.40 ± 0.08 nmol/mg, n = 27, and 33, respectively, $P < 0.0001$). This result confirmed the strong link between positive NADH fluorescence and the anaerobic state in frozen heart samples.

## Protocol 2

### Regional Coronary Blood Flow

In a preliminary study, the injection of microspheres (more than $1 \times 10^4$/g) into canine hearts to measure myocardial flow was shown to produce microspots of NADH fluorescence caused by microsphere embolization-induced ischemia,[22] indicating that the concomitant measurement of tissue flow in the hearts of animals treated with protocol 1 could not be accurately evaluated (Table 4). Therefore, we performed a separate but parallel protocol of NADH fluorescence study to analyze myocardial tissue flow using the microsphere method. The heart rates and mean aortic pressures were comparable with those in protocol 1 and did not change significantly throughout the experiment. Coronary inflow reductions were also comparable with those in protocol 1 (29.4 ± 5.2% in the endothelin group, and 30.0 ± 2.7% in the stenosis group, ns). Flow in myocardial tissue and the flow ratio in endo/epi tissues were not significantly reduced in either group, although the calculated subepicardial coronary vascular resistance was higher in the endothelin group than in the stenosis group. Neither the absolute flow value nor the endo/epi flow ratio were able to account for the larger ischemic areas observed in the endothelin group in protocol 1.

## DISCUSSION

Endothelin-1 directly constricts coronary smooth muscle and decreases blood flow, leading to severe myocardial ischemia; however the effects of ET-1 on myocardial ischemia in vivo have not been well characterized. This study produced the following findings: (1) ET-1 enlarged the myocardial ischemic area detected by NADH fluorescence, compared with that induced by similar reduction in coronary flow arising from stenosis. Moreover, ET-1 decreased the NAD/NADH ratio in both the subendocardium and the subepicardium, compared with the situation in the stenosis group, suggesting that ET-1 has flow-independent, direct pro-ischemic effects on myocytes in vivo. (2) ET-1 increased the coronary vascular resistance dominantly in the subepicardium and increased the ischemic area and the NADH content in the same region. These data suggest that ET-1 more selectively constricts subepicardial arterioles, extends myocardial ischemia transmurally, and causes an ST-elevation. (3) ET-1 generated smaller ischemic foci in the microcirculation than those generated by stenosis,

TABLE 2. Quantification of Ischemic Area and Transmural Distribution

| | Endothelin Group (n = 8) | | | Stenosis Group (n = 7) | | | Endothelin vs. Stenosis | |
|---|---|---|---|---|---|---|---|---|
| | Endo Mean (SD) | Epi Mean (SD) | Statistics | Endo Mean (SD) | Epi Mean (SD) | Statistics | Endo | Epi |
| Ischemic area | | | | | | | | |
| Endo or epi (%) | 66.3 (22.3) | 66.8 (23.3) | ns | 27.7 (27.2) | 8.5 (10.3) | $P = 0.03$ | $P = 0.01$ | $P < 0.0001$ |
| Total (%) | 66.4 (22.5) | | | 17.6 (18.2) | | | $P = 0.0005$ | |

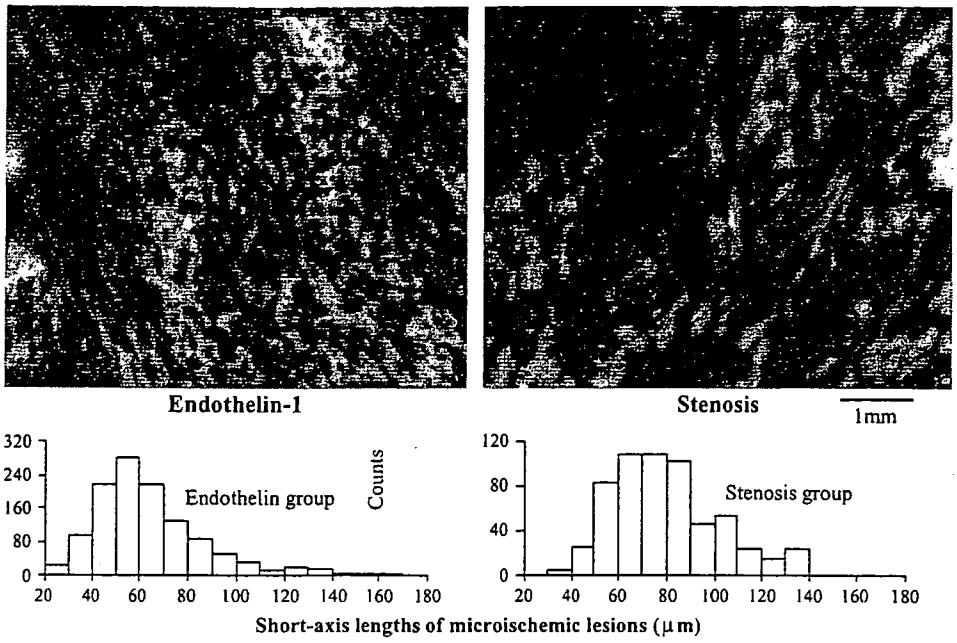


FIGURE 2. Magnified NADH fluorescence photographs (×100) showing microischemic foci in both the endothelin and stenosis groups. The histogram shows the distributions of the short-axis lengths of microischemic lesions in both groups. The endothelin group produced many similar shaped but smaller ischemic foci, compared with the stenosis group (61 ± 18 versus 76 ± 18 μm, $P < 0.0001$).

suggesting that the distal arteriolar levels of the coronary microcirculation may be affected by ET-1.

We found a clear dissociation between the reduction of coronary blood flow and the development of myocardial ischemia in the endothelin group, compared with the situation in the stenosis group. This finding was especially noticeable in the subendocardial region. In the endothelin group, we observed a subendocardial blood flow similar to that in the stenosis group, as detected using the non-radioisotope microsphere method. However, the ischemic area detected by NADH fluorescent was larger by more than two fold. This data clearly shows the flow-independent pro-ischemic effects of ET-1 in vivo. Although we did not clarify the direct mechanism of the pro-ischemic effects of ET-1 on myocytes, ET-1 may increase the oxygen demand of the myocytes. Previous reports have shown that endothelin-1 can increase intracellular $Ca^{2+}$ through the activation of voltage-dependent $Ca^{2+}$ currents[23,24] and can activate $Na^{+}$-$H^{+}$ exchange on isolated myocytes,[25] both of which produce inotropic effects and augment oxygen demand.[10,11] An increased left ventricular dP/dt following the intravenous administration of endothelin-1 was also reported in canine and rat model.[9,26] Furthermore, using an ex vivo Langendorff model of rat hearts, Grover et al[27] demonstrated the extension of myocardial ischemia in arrested heart, suggesting the pro-ischemic effect of endothelin-1. ET-1 was also reported to augment myocardial mitochondrial damage induced by rotenone; therefore, mitochondrial dysfunction during ischemia may also be enhanced by ET-1.[28] ET-1 can elicit the positive-inotropic effects by the cross-talk with norepinephrine and a release of norepinephrine in the operation may enhance the pro-ischemic effects of ET-1.[29] In this study, ET-1 did not change the heart rate or the myocardial ATP content; however, we speculate that positive inotropic effects associated with an enhanced metabolic demand or an aggravation of mitochondrial dysfunction may cause the pro-ischemic effects of ET-1.

Another interesting finding was the difference in the distribution of myocardial ischemia between the endothelin and stenosis groups. In the coronary stenosis group, both the reduction of tissue flow and the distribution of ischemia were

TABLE 3. Chemical Analyses of Myocardial Microsampling of Subendocardial or Subepicardial Layer in the Endothelin and Stenosis Groups

| | Endothelin Group | | | Stenosis Group | | | Endothelin vs. Stenosis | |
|---|---|---|---|---|---|---|---|---|
| | Endo Mean (SD) | Epi Mean (SD) | Statistics | Endo Mean (SD) | Epi Mean (SD) | Statistics | Endo | Epi |
| | n = 17 | n = 17 | | n = 14 | n = 14 | | | |
| NADH (nmol/mg) | 0.68 (0.25) | 0.67 (0.27) | ns | 0.5 (0.22) | 0.39 (0.08) | ns | $P = 0.048$ | $P = 0.001$ |
| NAD/NADH | 7.4 (2.9) | 7.6 (3.5) | ns | 10.9 (5.0) | 12.5 (2.6) | ns | $P = 0.02$ | $P = 0.0001$ |
| Lactate (nmol/mg) | 26.0 (12.9) | 28.8 (13.9) | ns | 31.0 (10.5) | 22.9 (8.5) | $P = 0.04$ | ns | ns |
| ATP (nmol/mg) | 42.8 (8.5) | 45.1 (11.1) | ns | 43.0 (6.9) | 41.7 (9.2) | ns | ns | ns |
| CP (nmol/mg) | 67.3 (27.7) | 74.7 (30.9) | ns | 63.4 (11.7) | 72.5 (20.3) | ns | ns | ns |

ATP, adenosine triphosphate; CP, creatine phosphate.

TABLE 4. Tissue Flow and Hemodynamics in the Stenosis and Endothelin Groups

| | Control Group Mean (SD) | Stenosis Group Mean (SD) | Endothelin Group Mean (SD) | ANOVA |
|---|---|---|---|---|
| CVR (mm Hg/mL/min/g) | | | | |
| Endo | 134 (48) | 100 (35) | 161 (90) | ns |
| Epi | 118 (56) | 67* (16) | 160* (86) | $P = 0.03$ |
| Tissue flow (mL/min/g) | | | | |
| Endo | 0.93 (0.29) | 0.71 (0.23) | 0.97 (0.53) | ns |
| Epi | 1.14 (0.43) | 1.01 (0.27) | 0.86 (0.31) | ns |
| Heart rate (/min) | 180 (13) | 180 (12) | 181 (13) | Ns |
| mAOP (mm Hg) | 115 (15) | 115 (15) | 117 (14) | Ns |
| mCPP (mm Hg) | 117† (13) | 65†‡ (13) | 119‡ (15) | $P < 0.0001$ |

CVR, coronary vascular resistance; mAOP, mean aortic pressure; mCPP, mean coronary perfusion pressure (n = 7).
*Stenosis group vs. endothelin group: $P = 0.0093$; †Control group vs. stenosis group: $P < 0.0001$; ‡Stenosis group vs. endothelin group: $P < 0.0001$.

predominant in the subendocardium. ET-1 administration, however, significantly increased the subepicardial coronary vascular resistance. The increase in the ST-elevation by ET-1 could be due to the transmural development of myocardial ischemia, because subepicardial ischemia widens the solid angle of the subepicardial electrode toward the ischemia front, resulting in an increase in the ST-segment.[30] A decrease in subepicardial blood flow induced by ET-1 was also reported by Clozel[31] and Ricou.[32] Although the precise mechanism for the change in the coronary flow distribution induced by ET-1 remains unclear, differences in the transmural distributions or affinities of the ET-1 receptor or the target molecules of ET-1 (for example, ATP-sensitive potassium channels) may explain this interesting phenomenon.[33,34]

Karwatovska-Prokopczuk et al[5] challenged the comparison of endothelin-induced and mechanically induced flow reductions in Langendorff-perfused rabbit hearts, claiming that ET-1 did not exacerbate ischemia. They assessed myocardial ischemia by evaluating oxygen consumption, pH, and purine bodies in the coronary sinus blood. We observed the selective vasoconstriction in the subepicardium using NADH fluorescence; therefore, it might be difficult to assess myocardial ischemia by examining coronary sinus blood. We also tried to measure arterio-venous differences in oxygen and lactate in the coronary circulation but could not identify any ischemia severity between the two treatment groups (data not shown). We also found that some indicators of myocardial ischemia, such as the lactate or creatine phosphate content, were similar in the two treatment groups. Because an increase in NADH and a decrease in the NAD/NADH ratio are the most rapid and sensitive markers for the ischemic redox changes, the method used in the present study can clarify the extent and severity of metabolic changes with a higher sensitivity.

The third unique effect of ET-1 was the appearance of making smaller ischemic foci in the microcirculation, compared with these observations in the stenosis model, as detected by the visualization of many spindle-shaped microischemic foci. Because ET-1 constricts more distal arterioles, as reported by microscopic observation of narrowing small vessels, ET-1 can dominantly regulate coronary microcirculation.[35,36] Under the low flow condition induced by stenosis, subepicardial arteries are maximally dilated, preventing the extension of ischemia. However, the systolic compression of subendocardial arteries limits this compensatory mechanism and induces subendocardial ischemia. A similar size of microischemia was observed in a hemorrhagic shock model.[22]

## CONCLUSION

Endothelin-1 produced a larger ischemic area than stenosis in the presence of equivalent reduction in coronary inflow. The mechanism for ET-1–induced ischemia might depend on direct pro-ischemic effects on myocytes and vasoconstriction of the coronary microcirculation, predominantly in the subepicardium in vivo.

## ACKNOWLEDGMENTS

*The authors thank Mr. Yozo Ohnishi in the Faculty of Medical Equipment of Keio University for his dedicated and excellent technical support and Dr. Motoaki Bessho of the Eisai Tokyo Laboratory for his excellent support in analysis of the metabolites in the myocardial tissues. We also appreciate Mr. Wataru Kawamura of Karl Zeiss Vision Co. Ltd. for his support in analyzing the size of the microischemic foci.*

## REFERENCES

1. Yanagisawa M, Kurihara H, Kimura S, et al. A novel potent vasoconstrictor peptide produced by vascular endothelial cells. *Nature.* 1988;232:411–415.
2. Igarashi Y, Aizawa Y, Tamura M, et al. Vasoconstrictor effect of endothelin on the canine coronary artery: Is a novel endogenous peptide involved in regulating myocardial blood flow and coronary spasm. *Am Heart J.* 1989;118:674–678.
3. Vojacek J, Kolar J, Lisy O, et al. Time course of endothelin-1 plasma level in patients with acute coronary syndromes. *Cardiology.* 1999;91:114–118.
4. Muramatsu K, Tomoike H, Ohara Y, et al. Effects of endothelin-1 on epicardial coronary tone, coronary blood flow, ECG-ST change and regional wall motion in anesthetized dogs. *Heart Vessels.* 1991;6:191–196.
5. Karwatowska-Prokopczuk E, Wennmalm Å. Effects of endothelin on coronary flow, and mechanical performance, oxygen uptake, and formation of purines and on outflow of prostacyclin in the isolated rabbit heart. *Circ Res.* 1990;66:46–54.
6. Fukuda K, Hori S, Kusuhara M, et al. Intracoronary endothelin-1 increases coronary retrograde pressure by constricting arterioles. *Cardiovasc Res.* 1990;24:987–992.

7. Watanabe T, Suzuki N, Shimamoto N, et al. Endothelin in myocardial infarction. *Nature*. 1990;344:114.
8. Grover GJ, Dzwonczyk S, Parham CS. The endothelin-1 receptor antagonist BQ-123 reduces infarct size in a canine model of coronary occlusion and reperfusion. *Cardiovasc Res*. 1993;27:1613–1618.
9. Kitayoshi T, Watanabe T, Shimamoto N. Cardiovascular effects of endothelin in dogs: positive inotropic action in vivo. *Eur J Pharmacol*. 1989;166:519–522.
10. Ishikawa T, Yanagisawa M, Kimura S, et al. Positive inotropic action of novel vasoconstrictor peptide endothelin on guinea pig atria. *Am J Physiol*. 1988;255:H970–H973.
11. Takahashi M, Endoh M. Characterization of positive inotropic effect of endothelin on mammalian ventricular myocardium. *Am J Physiol*. 1991; 261:H611–H619.
12. Maczewski M, Beresewicz A. The role of endothelin, protein kinase C and free radicals in the mechanism of the post-ischemic endothelial dysfunction in guinea-pig hearts. *J Mol Cell Cardiol*. 2000;32:297–310.
13. Bessho M, Tajima T, Hori S, et al. NAD and NADH values in rapidly sampled dog heart tissues by two different extraction methods. *Anal Biochem*. 1989;182:304–308.
14. Hori S, Nakazawa H, Ohnishi Y, et al. A rapid cross-sectioning and freeze-clamping device for the beating canine heart. *J Mol Cell Cardiol*. 1989;21: 203–210.
15. Kurihara H, Yamaoki K, Nagai R, et al. Endothelin: a potent vasoconstrictor associated with coronary vasospasm. *Life Sci*. 1989;44: 1937–1943.
16. Barlow CD, Chance B. Ischemic areas in perfused rat heart: measured by NADH fluorescence photography. *Science*. 1976;193:909–910.
17. Chance B, Williamson JR, Jamieson D, et al. Properties and kinetics of reduced pyridine nucleotide fluorescence of the isolated and in vivo rat heart. *Biochem Z*. 1965;341:357–377.
18. Karp MT, Rauniop RP, Lovgren TN-E. Simultaneous extraction and combined bioluminescent assay of NAD+ and NADH. *Anal Biochem*. 1983;128:175–180.
19. Shimojo N, Naka K, Nakajima C, et al. Test-strip method for measuring lactate in whole blood. *Clin Chem*. 1989;35:1992–1994.
20. Lowry OH, Rosebrough NJ, Farr AL. Protein measurement with the Folin phenol reagent. *J Biochem*. 1951;193:265–275.
21. Mori H, Haruyama S, Shinozaki Y, et al. New nonradioactive microspheres and more sensitive X-ray fluorescence to measure regional blood flow. *Am J Physiol*. 1992;263:H1946–H1957.
22. Miyazaki K, Hori S, Inoue S, et al. Characterization of energy metabolism and blood flow distribution in myocardial ischemia in hemorrhagic shock. *Am J Physiol*. 1997;273:H600–H607.
23. Xu Y, Sandirasegarane L, Gopalakrishnan V. Protein kinase C inhibitors enhance endothelin-1and attenuate vasopressin and angiotensin II evoked [Ca2+] i elevation in the rat cardiomyocyte. *Br J Pharmacol*. 1993;108: 6–8.
24. Lauer MR, Gunn MD, Clusin WT. Endothelin activates voltage dependent Ca2+ current by a G protein-dependent mechanism in rabbit cardiac myocytes. *J Physiol*. 1992;448:729–747.
25. Khandoudi N, Ho J, Karamazyn M. Role of Na+-H+ exchange in mediating effects of endothelin-1 on normal and ischemic/reperfused hearts. *Circ Res*. 1994;75:369–378.
26. Beyer ME, Slesak G, Nerz S, et al. Effects of endothelin-1 and URL 1620 on myocardial contractility and myocardial energy metabolism. *J Cardiovasc Pharmacol*. 1995;26(Suppl 3):S150–S152.
27. Grover GJ, Sleph PG, Fox M, et al. Role of endothelin-1 and big endothelin-1 in modulating coronary vascular tone, contractile function and severity of ischemia in rat hearts. *J Pharmacol Exp Ther*. 1992;263: 1074–1082.
28. Yuki K, Suzuki T, Katoh S, et al. Endothelin-1 stimulates cardiomyocyte injury during mitochondrial dysfunction in culture. *Eur J Pharmacol*. 2001;431:163–170.
29. Chu L, Takahashi R, Norota I, et al. Signal transduction and Ca2+ signaling in contractile regulation induced by crosstalk between endothelin-1 and norepinephrine in dog ventricular myocardium. *Circ Res*. 2003;92:1024–1032.
30. Holland RP, Arnsdorf MF. Solid angle theory and the electrocardiogram: physiologic and quantitative interpretations. *Prog Cardiovasc Dis*. 1977; 19:431–457.
31. Clozel JP, Clozel M. Effect of endothelin on the coronary vascular bed in open-chest dogs. *Circ Res*. 1989;65:1193–1200.
32. Ricou FJ, Murata K, Oh B-H, et al. Evaluation of inotropic effect of endothelin-1 in vivo. *J Cardiovasc Pharmacol*. 1992;20:671–677.
33. Furukawa T, Kimura S, Furukawa N, et al. Role of cardiac ATP-regulated potassium channels in differential responses of endocardial and epicardial cells to ischemia. *Circ Res*. 1991;68:1693–1702.
34. Miyoshi Y, Nakaya Y, Wakatsuki T, et al. Endothelin blocks ATP-sensitive K+ channels and depolarizes smooth muscle cells of porcine coronary artery. *Circ Res*. 1992;70:612–616.
35. Marcus M, Chilian WM, Kanatsuka H, et al. Understanding the coronary circulation through studies at the microvascular level. *Circulation*. 1990; 82:1–7.
36. Wan W, Kanatsuka H, Akai K, et al. Effects of low doses of endothelin-1 on basal vascular tone and autoregulatory vasodilatation in canine coronary microcirculation in vivo. *Jpn Circ*. 1999;63:617–623.

Japanese Journal of Applied Physics
Vol. 44, No. 1A, 2005, pp. 446–449



# Quasi-Monochromatic X-Ray Generator Utilizing Graphite Cathode Diode with Transmission-Type Molybdenum Target

Michiaki SAGAE, Eiichi SATO, Etsuro TANAKA[1], Yasuomi HAYASI, Hidezo MORI[2], Toshiaki KAWAI[3], Toshio ICHIMARU[4], Shigehiro SATO[5], Kazuyoshi TAKAYAMA[6] and Hideaki IDO[7]

*Department of Physics, Iwate Medical University, 3-16-1 Honchodori, Morioka 020-0015, Japan*
[1]*Department of Nutritional Science, Faculty of Applied Bio-science, Tokyo University of Agriculture, 1-1-1 Sakuragaoka, Setagaya-ku 156-8502, Japan*
[2]*Department of Cardiac Physiology, National Cardiovascular Center Research Institute, 5-7-1 Fujishiro-dai, Suita, Osaka 565-8565, Japan*
[3]*Electron Tube Division #2, Hamamatsu Photonics K.K., 314-5 Shimokanzo, Toyooka Village, Iwata-gun 438-0193, Japan*
[4]*Department of Radiological Technology, School of Health Sciences, Hirosaki University, 66-1 Honcho, Hirosaki 036-8564, Japan*
[5]*Department of Microbiology, School of Medicine, Iwate Medical University, 19-1 Uchimaru, Morioka 020-8505, Japan*
[6]*Shock Wave Research Center, Institute of Fluid Science, Tohoku University, 2-1-1 Katahira, Aoba-ku, Sendai 980-8577, Japan*
[7]*Department of Applied Physics and Informatics, Faculty of Engineering, Tohoku Gakuin University, 1-13-1 Chuo, Tagajo 985-8537, Japan*

(Received June 19, 2004; accepted October 15, 2004; published January 11, 2005)

An X-ray generator consists of a negative high-voltage power supply and a field-emission-type cold-cathode X-ray tube. The tube is a glass-enclosed diode utilizing a transmission-type molybdenum target with a thickness of 20 μm, a needle graphite (carbon) cathode, a glass tube body, and a 0.5-mm-thick beryllium window. The tube current decreases gradually with time. After aging for 30 minutes, the tube current was approximately 0.2 mA with a tube voltage of 25 kV, and the focal-spot dimensions were 2.2 × 1.6 mm. Characteristic X-rays of molybdenum K-series were obtained after penetrating the molybdenum target and the beryllium window, and the K-absorption edge was observed clearly. The generator produced number of K photons was approximately $4 \times 10^6$ photons/cm$^2$·s at 1.0 m from the source. The average photon energies of Kα and Kβ lines were 17.4 and 19.6 keV, respectively, and quasi-monochromatic radiography was performed using a computed radiography system. [DOI: 10.1143/JJAP.44.446]

KEYWORDS: quasi-monochromatic X-rays, characteristic molybdenum X-rays, field emission, transmission target, quasi-monochromatic radiography

## 1. Introduction

Conventional medical X-ray tubes enable the observation of parts of the inside of the human body that cannot be seen by other ways. The X-ray images obtained with these tubes are exposed by both the bremsstrahlung and characteristic X-rays, unless monochromatic radiography is specifically performed. Monochromatic parallel X-ray beams are produced by synchrotrons using single crystals, and these beams have been employed to perform enhanced K-edge angiography[1–3] and X-ray phase imaging.[4,5] Subsequently, monochromatic X-ray computed tomography at two different energies has provided information on the electron density of human tissue.[6] In addition, a compact pulsed tunable monochromatic X-ray source has been designed, developed, and tested.[7] From the source, conical X-ray beams from 10 to 50 keV with pulse widths of 8 ps have been produced, and these beams are useful for biomedical imaging and protein crystallography.

Currently, flash X-ray generators[8–12] utilize cold-cathode radiation tubes and produce extremely high-dose-rate X-ray pulses with durations of less than 1 μs. In order to produce monochromatic X-rays, plasma flash X-ray generators are useful, since intense and sharp characteristic X-rays have been produced from weakly ionized linear plasmas of nickel,[13] copper[14] and molybdenum,[15] while bremsstrahlung rays are rarely detected.

In order to produce steady-state X-rays using a cold-cathode tube, the combination of the target and cathode electrodes is a very important factor. In view of the cathode, a carbon nanotube[16] is a useful field emitter and can be used as a cold cathode in an X-ray tube. Without using nanotubes, electrons can be emitted comparatively easily when lines of electric force are concentrated on a needle tip. Characteristic K-series X-rays have been obtained using a filter made of the same element as the target.

In the present research, we developed a cold-cathode X-ray tube with a needle-shaped graphite cathode, and applied it to produce characteristic molybdenum K-series X-rays by uisng a transmission target.

## 2. Generator

Figure 1 shows the block diagram of the X-ray generator, which consists of a negative high-voltage power supply (Model 500, −100 kV-3 mA, Pulse Electric Eng. Inc.) with dimensions of 450 × 430 × 150 mm and an X-ray tube. In the X-ray tube, the negative high voltage is applied to the cathode electrode, and the anode (target) is connected to the ground potential.

The X-ray tube is a cold-cathode diode type, as illustrated in Fig. 2. In order to perform soft radiography, including mammography, we developed a quasi-monochromatic X-ray tube with a molybdenum target. This tube consists of the following major devices: a needle-shaped graphite cathode with a tip angle of 54° and a diameter of 3.0 mm, a

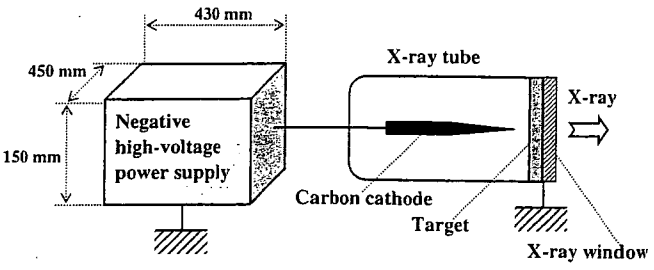


Fig. 1. Block diagram of quasi-monochromatic X-ray generator with cold-cathode diode.

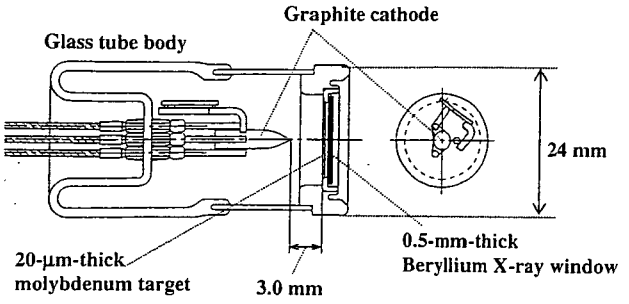


Fig. 2. Structure of X-ray tube.

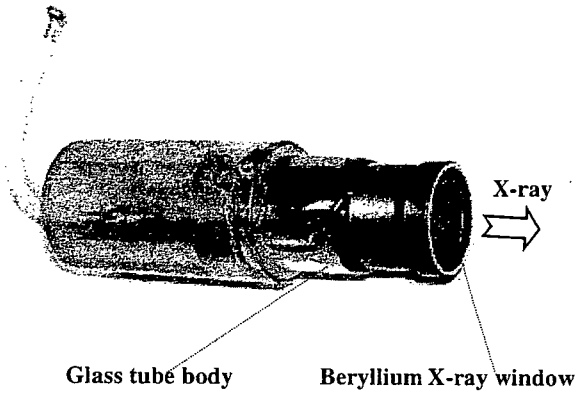


Fig. 3. Cold-cathode X-ray tube with transmission-type molybdenum target.

molybdenum disk target 20 μm thick, and a glass tube body. The target-cathode distance is 3.0 mm, and the transmission X-rays are obtained after the beam passes through the target and a 0.5-mm-thick beryllium X-ray window (Fig. 3). In this case, since the target plays the role of a K-edge filter for effectively absorbing bremsstrahlung X-rays with energies higher than the K-absorption edge, characteristic K-series X-rays are produced. The pressure in the glass-enclosed tube is primarily determined by the pressure when evacuation is stopped, and is approximately $1 \times 10^{-4}$ Pa. The tube voltage is always constant and is regulated by the constant voltage power supply. Subsequently, the tube current is primarily determined by the tube voltage and the target-cathode distance, and increases with decreasing distance and increasing voltage.

In this experiment, the tube voltage applied was from 20 to 30 kV, and the exposure time was controlled in order to obtain optimum X-ray intensity for radiography.

## 3. Characteristics

### *3.1 X-ray intensity*

In the field emission X-ray tube, it was very difficult to measure the X-ray intensity correctly, since the intensity gradually decreased during exposure, and small-scale vacuum breakdown may often occur. The X-ray intensity was measured using a Solidose 308 M ionization chamber for mammography at 1.0 m from the X-ray source with an exposure time of 10 s. Because the tube current increased when the tube voltage was increased, the X-ray intensity increased substantially with increasing tube voltage. In this measurement, the intensity rate with a tube voltage of 25 kV was approximately 0.3 μC/kg·s (=10 μJ/kg·s = 10 μGy/s) at 1.0 m from the source.

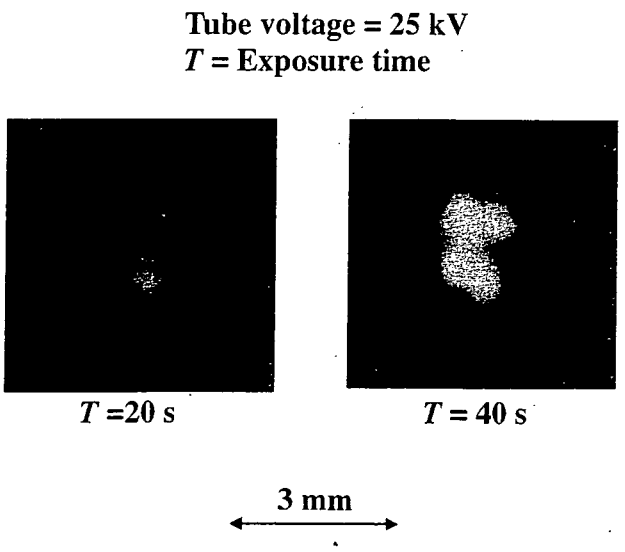


Fig. 4. Images of X-ray source with changes in exposure time.

### *3.2 X-ray source*

In order to measure the images of the X-ray source, we employed a pinhole camera with a hole diameter of 100 μm in conjunction with a Polaroid XR-7 (film). When the exposure time was increased with a tube voltage of 25 kV, the spot intensity increased, but the spot dimensions seldom varied and had values of 2.2 × 1.6 mm (Fig. 4).

### *3.3 Cathode voltage and tube current*

Cathode voltage and tube current were measured using a high-voltage divider and a resistor, respectively (Figs. 5 and 6). In this generator, the cathode voltage is −1 times the tube voltage, and we observed stable cathode voltages. Thereafter, the tube current increased exponentially with increasing tube voltage in a short time. In addition, the current was unstable, and decreased gradually with time.

### *3.4 X-ray spectra*

X-ray spectra were measured using a transmission-type spectrometer with a curved lithium fluoride crystal 0.5 mm thick. The spectra were taken using a computed radiography (CR) system (Konica Regius 150)[17] with a wide dynamic range, and relative X-ray intensity was calculated from Dicom digital data. Figure 7 shows the measured spectra from the transmission-type molybdenum target. We observed lines of characteristic K-series X-rays and K-absorption edges of molybdenum. The characteristic X-ray intensity of the Kα and Kβ lines increased substantially when the tube voltage was increased.

## 4. Radiography

Radiography was performed using the CR system with a sampling pitch of 87.5 μm. The distance between the X-ray source and the imaging plate was 1.0 m.

Spatial resolution was roughly measured using wires. Radiograms of tungsten wires coiled around a pipe made of polymethyl methacrylate are shown in Fig. 8. Although the

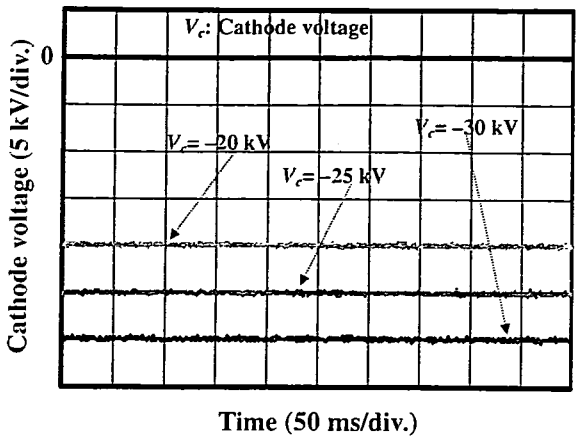


Fig. 5. Cathode voltages.

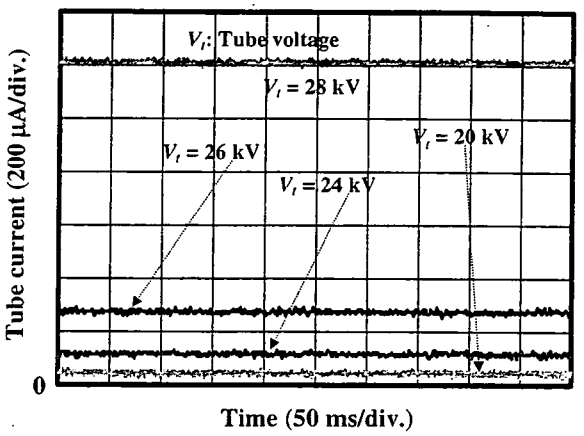


Fig. 6. Tube currents.

image contrast decreased somewhat with decreasing wire diameter due to blurring of the image caused by the sampling pitch, a 50-μm-diameter wire could be observed.

Figures 9 and 10 show angiograms of hearts. Iodine-based microspheres of 15 μm in diameter were used, and coronary

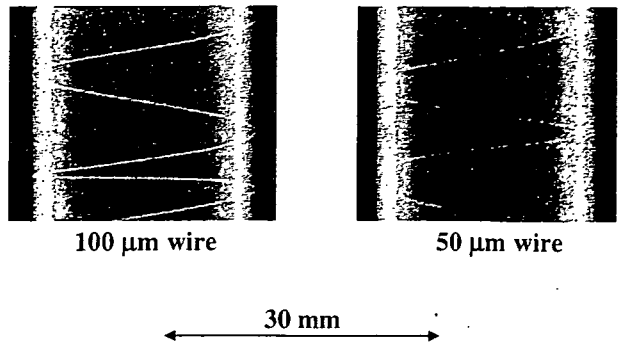


Fig. 8. Radiograms of tungsten wires of 50 and 100 μm diameter coiled around a pipe made of polymethyl methacrylate with tube voltage of 25 kV and exposure time of 20 s.

arteries and fine blood vessels of approximately 100 μm diameter were visible.

## 5. Discussion

In summary, we developed a simple X-ray generator with the cold-cathode diode and succeeded in producing characteristic molybdenum K-series X-rays using the transmission target as the K-edge filter. Subsequently, we confirmed the filtering effect of the target, and bremsstrahlung X-rays with photon energies higher than the edge were rarely detected with a tube voltage of 23 kV.

The current density $J$ (A/cm$^2$) under field emission is written as:

$$J = 1.54 \times 10^{-6}(V/d)^2 \cdot \exp(-6.8 \times 10^7 \phi^{1.5} d/V)/\phi, \quad (1)$$

where $V$ (V) is the tube voltage, $d$ (cm) is the target-cathode distance, and $\phi$ (V) is the work function of the cathode element. Therefore, the current values in Fig. 6 corresponded qualitatively to eq. (1).

During the X-ray exposure, although the tube current decreases slightly due to ion sputtering, stable current flow can be obtained by selecting the appropriate cathode material and by controlling the radius of curvature of the cathode tip. In addition, the generator-produced number of

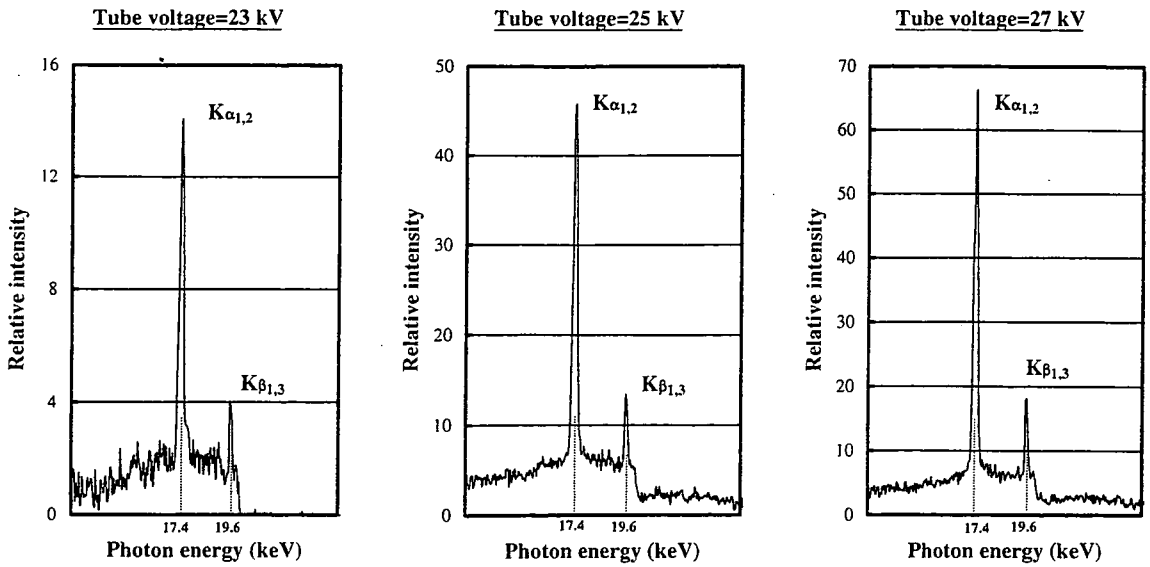


Fig. 7. X-ray spectra.

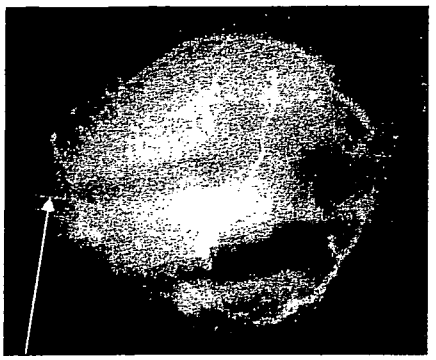


Fig. 9. Angiogram, using iodine microspheres, of extracted rabbit heart. Tube voltage and exposure time were 25 kV and 20 s, respectively.

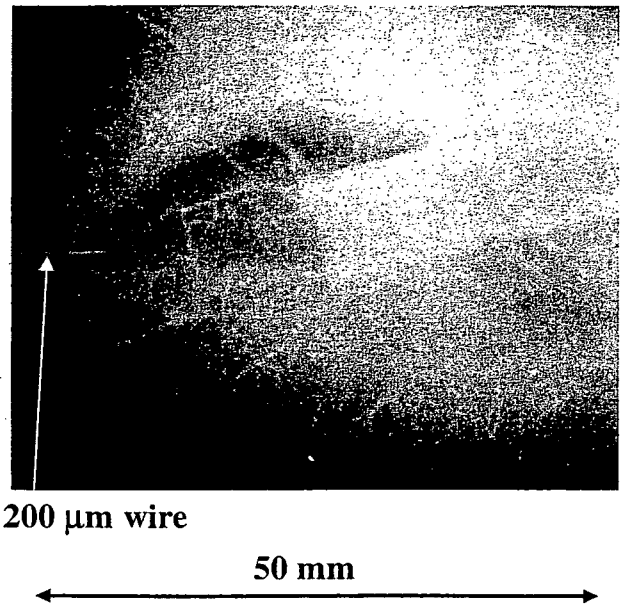


Fig. 10. Angiogram of extracted dog heart with tube voltage of 25 kV and exposure time of 60 s.

characteristic photons was approximately $4 \times 10^6$ photons/$cm^2 \cdot s$ at 1.0 m from the source with a tube voltage of 25 kV, and the photon count rate could be increased easily by increasing the tube voltage and current.

The focal spot dimensions decrease with decreasing target-cathode space, and the distance between the X-ray source and the imaging plate should be increased as much as possible to improve the spatial resolution. In soft radiography achieved with characteristic molybdenum K-series X-rays, because an X-ray lens such as a polycapillary plate[18] can be employed, the spatial resolution may be improved by decreasing the inner capillary diameter.

Under the pulsed operation, the high-voltage durability increases substantially, and both the size of the X-ray tube and the diameter of the high-voltage coaxial cable can be decreased. In this case, because the time-average tube current is regulated by the pulse repetition rate, both the tube voltage and the current can be controlled without using a hot cathode.

Recently, we developed a cerium-target X-ray tube to perform enhanced K-edge angiography utilizing cerium K$\alpha$ rays (34.6 keV), since the rays are absorbed effectively by iodine-based contrast media with a K-edge of 33.2 keV. In addition, K$\alpha$ rays from ytterbium (52.0 keV), tantalum (57.1 keV), and tungsten (58.9 keV) targets are very useful for performing K-edge angiography using gadolinium-based contrast media with an edge of 50.2 keV. Hence, using these rays, because the absorbed dose can be decreased effectively, extremely low-dose angiography can be accomplished.

## Acknowledgment

This work was supported by Grants-in-Aid for Scientific Research (13470154, 13877114, and 16591222) and Advanced Medical Scientific Research from MECSST, Grants from Keiryo Research Foundation, The Promotion and Mutual Aid Corporation for Private Schools of Japan, JST, NEDO, and MHLW (HLSRG, RAMT-nano-001, RHGTEFB-genome-005, and RGCD13C-1).

1) A. C. Thompson, H. D. Zeman, G. S. Brown, J. Morrison, P. Reiser, V. Padmanabahn, L. Ong, S. Green, J. Giacomini, H. Gordon and E. Rubenstein: Rev. Sci. Instrum. **63** (1992) 625.
2) H. Mori *et al.*: Radiology **201** (1996) 173.
3) K. Hyodo, M. Ando, Y. Oku, S. Yamamoto, T. Takeda, Y. Itai, S. Ohtsuka, Y. Sugishita and J. Tada: J. Synchrotron Rad. **5** (1998) 1123.
4) T. J. Davis, D. Gao, T. E. Gureyev, A. W. Stevenson and S. W. Wilkims: Nature **373** (1995) 595.
5) A. Momose, T. Takeda, Y. Itai and K. Hirano: Nature Medicine **2** (1996) 473.
6) M. Torikoshi, T. Tsunoo, M. Sasaki, M. Endo, Y. Noda, T. Kohno, K. Hyodo, K. Uesugi and N. Yagi: Phys. Med. Biol. **48** (2003) 673.
7) F. E. Carroll, M. H. Mendenhall, R. H. Traeger, C. Brau and J. W. Waters: Am. J. Roentgenol. **181** (2003) 1197.
8) R. Germer: J. Phys. E: Sci. Instrum. **12** (1979) 336.
9) E. Sato, H. Isobe and F. Hoshino: Rev. Sci. Instrum. **57** (1986) 1399.
10) A. Shikoda, E. Sato, M. Sagae, T. Oizumi, Y. Tamakawa and T. Yanagisawa: Rev. Sci. Instrum. **65** (1994) 850.
11) K. Takahashi, E. Sato, M. Sagae, T. Oizumi, Y. Tamakawa and T. Yanagisawa: Jpn. J. Appl. Phys. **33** (1994) 4146.
12) E. Sato, K. Takahashi, M. Sagae, S. Kimura, T. Oizumi, Y. Hayasi, Y. Tamakawa and T. Yanagisawa: Med. & Biol. Eng. & Comput. **32** (1994) 289.
13) E. Sato, Y. Hayasi, R. Germer, E. Tanaka, H. Mori, T. Kawai, T. Ichimaru, S. Sato, K. Takayama and H. Ido: J. Electron Spectrosc. & Related Phenom. **137–140** (2004) 713.
14) E. Sato, Y. Hayasi, R. Germer, E. Tanaka, H. Mori, T. Kawai, T. Ichimaru, K. Takayama and H. Ido: Rev. Sci. Instrum. **74** (2003) 5236.
15) E. Sato, Y. Hayasi, R. Germer, E. Tanaka, H. Mori, T. Kawai, H. Obara, T. Ichimaru, K. Takayama and H. Ido: Jpn. J. Med. Phys. **20** (2003) 123.
16) H. Sugie, M. Tanemura, V. Filip, K. Iwata, K. Takahashi and F. Okuyama: Appl. Phys. Lett. **78** (2000) 2578.
17) E. Sato, K. Sato and Y. Tamakawa: Ann. Rep. Iwate Med. Univ. Sch. Lib. Arts Sci. **35** (2000) 13.
18) E. Sato, Y. Hayasi, R. Germer, E. Tanaka, H. Mori, T. Kawai, T. Ichimaru, S. Sato, K. Takayama and H. Ido: J. Electron Spectrosc. Related Phenom. **137–140** (2004) 705.

Japanese Journal of Applied Physics
Vol. 44, No. 11, 2005, pp. 8204–8209



# Variations in Cerium X-ray Spectra and Enhanced K-Edge Angiography

Eiichi SATO, Etsuro TANAKA[1], Hidezo MORI[2], Toshiaki KAWAI[3], Takashi INOUE[4], Akira OGAWA[4], Akira YAMADERA[5], Shigehiro SATO[6], Fumihito ITO[7], Kazuyoshi TAKAYAMA[8], Jun ONAGAWA[9] and Hideaki IDO[9]

*Department of Physics, Iwate Medical University, 3-16-1 Honchodori, Morioka, Iwate 020-0015, Japan*
[1]*Department of Nutritional Science, Faculty of Applied Bio-science, Tokyo University of Agriculture, 1-1-1 Sakuragaoka, Setagaya-ku, Tokyo 156-8502, Japan*
[2]*Department of Cardiac Physiology, National Cardiovascular Center Research Institute, 5-7-1 Fujishiro-dai, Suita, Osaka 565-8565, Japan*
[3]*Electron Tube Division #2, Hamamatsu Photonics K.K., 314-5 Shimokanzo, Iwata, Shizuoka 438-0193, Japan*
[4]*Department of Neurosurgery, School of Medicine, Iwate Medical University, 19-1 Uchimaru, Morioka 020-8505, Japan*
[5]*Department of Radiological Technology, School of Health Sciences, Hirosaki University, 66-1 Honcho, Hirosaki, Aomori 036-8564, Japan*
[6]*Department of Microbiology, School of Medicine, Iwate Medical University, 19-1 Uchimaru, Morioka 020-8505, Japan*
[7]*Digital Culture Technology Corp., Kanno The 2nd Bldg., 3-17-7 Chuo-dori, Morioka 020-0021, Japan*
[8]*Shock Wave Research Center, Institute of Fluid Science, Tohoku University, 2-1-1 Katahira, Aoba-ku, Sendai 980-8577, Japan*
[9]*Department of Applied Physics and Informatics, Faculty of Engineering, Tohoku Gakuin University, 1-13-1 Chuo, Tagajo, Miyagi 985-8537, Japan*

(Received March 31, 2005; accepted July 15, 2005; published November 9, 2005)

A cerium-target X-ray tube is useful in performing cone-beam K-edge angiography because K-series characteristic X-rays from the cerium target are absorbed effectively by iodine-based contrast media. The X-ray generator consists of a main controller and a unit with a high-voltage circuit and a fixed anode X-ray tube. The tube is a 1.0-mm-focus diode with a cerium target and a 0.5-mm-thick beryllium window. The maximum tube voltage and current were 65 kV and 0.4 mA, respectively. Cerium Kα rays were selected out using a barium sulfate filter, and the X-ray intensities without filtering and with a barium sulfate filter were 209 and 16.8 μGy/s, respectively, at 1.0 m from the source with a tube voltage of 60 kV and a current of 0.40 mA. Angiography was performed with an X-ray film using the filter and iodine-based microspheres 15 μm in diameter. In the angiography of nonliving animals, we observed fine blood vessels approximately 100 μm in diameter with high contrasts.
[DOI: 10.1143/JJAP.44.8204]

KEYWORDS: X-ray tube, cerium target, monochromatic X-rays, Kα rays, K-edge angiography

## 1. Introduction

Monochromatic parallel X-ray beams have been used to perform enhanced K-edge angiography[1–4] using iodine-based contrast media because the X-rays with photon energies of approximately 35 keV are absorbed easily by iodine with a K-edge of 33.2 keV. In conjunction with a high-resolution camera, fine blood vessels of approximately 50 μm can be observed.[3] Although the parallel beams have also been employed to perform phase-contrast radiography,[5–7] weakly absorbing materials have been observed with high contrasts.

Flash radiography of biomedical tissues has been investigated for a number of years, and several different flash X-ray generators have been developed corresponding to specific radiographic objectives.[8–11] The advantages of flash radiography include the use of K-series characteristic X-rays and their relatively good imaging contrast. However, monochromatic flash radiography[12–15] has encountered difficulties in increasing X-ray duration, and in performing X-ray computed tomography (CT).

Recently, a steady-state X-ray generator utilizing a cerium-target tube[16] has been developed, and has been employed to perform enhanced K-edge angiography achieved with cerium Kα rays and iodine-based contrast media, since Kα rays (34.6 keV) are absorbed effectively by iodine. In this case, because the sampling pitch of a computed radiography system (Konica Minolta Regius 150)[17] is 87.5 μm, a spatial resolution of approximately 100 μm has been obtained. Therefore, the resolution should be minimized by using a film or decreasing the pitch.

In the above-mentioned preliminary experiment,[16] we employed a cadmium tellurium detector with a photon energy resolution of 1.7 keV to measure X-ray spectra from the cerium target. However, the resolution should be minimized to measure the characteristic X-ray intensity and to confirm the K-edge effect of a barium sulfate filter for absorbing Kβ and bremsstrahlung X-rays, because the photon energy width of the K-series lines is approximately 1 keV.

In the present research, we measured the X-ray spectra from a cerium target tube using a germanium detector with a photon energy resolution of 0.12 keV and performed a preliminary study on enhanced K-edge angiography achieved with cerium Kα rays.

## 2. Generator

Figure 1 shows a block diagram of the X-ray generator, which consists of a main controller and an X-ray tube unit

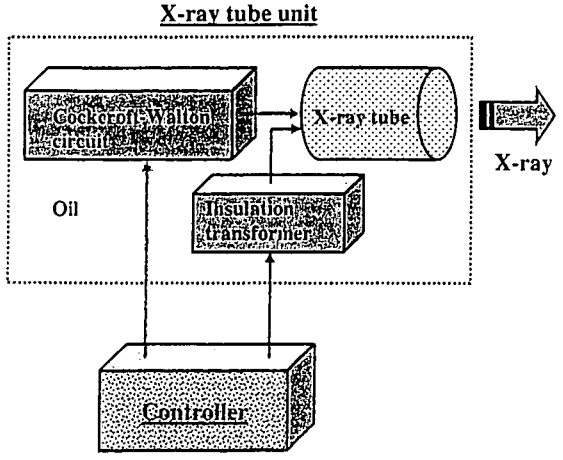


Fig. 1. Block diagram of compact X-ray generator with cerium-target radiation tube, which is used particularly for K-edge angiography using iodine-based contrast media.

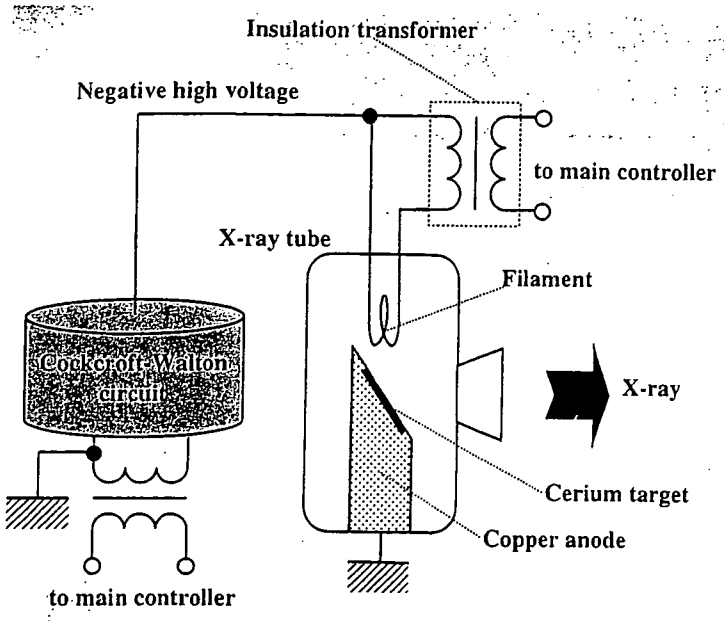


Fig. 2. Main circuit of X-ray generator.

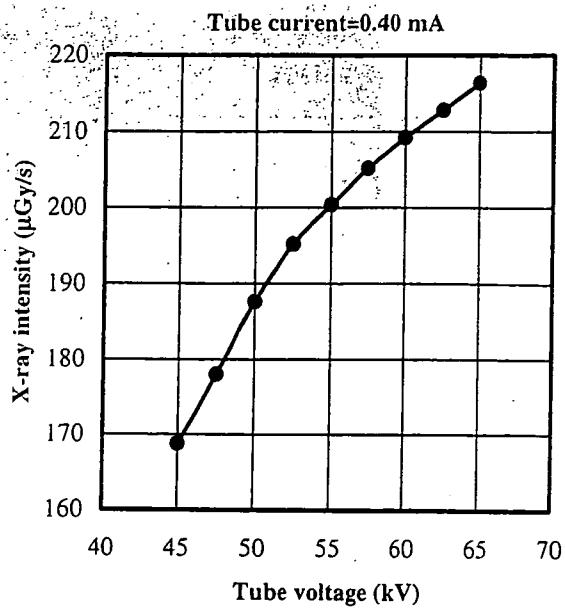


(a)

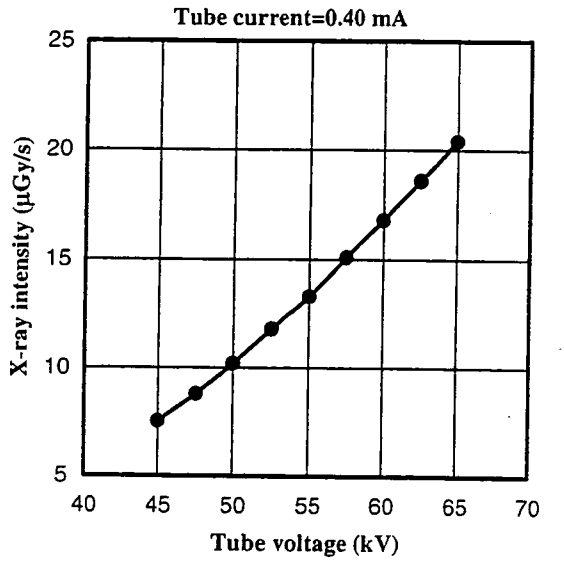


(b)

Fig. 3. X-ray intensity measured at 1.0 m from X-ray source according to changes in tube voltage (a) without filtering and (b) using barium-sulfate filter.

with a Cockcroft–Walton circuit and a cerium-target tube. The tube voltage, the current, and the exposure time can be controlled by the controller. The main circuit for producing X-rays is illustrated in Fig. 2, and it employed the Cockcroft–Walton circuit in order to decrease the dimensions of the tube unit. In the X-ray tube, a high negative voltage is applied to the cathode electrode, and the anode (target) is connected to the tube unit case (ground potential) to cool the anode and the target effectively. The filament heating current is supplied by an AC power supply in the controller in conjunction with an insulation transformer. The tube is a conventional diode with a plate cerium target, a 1.0 mm focus, a take-off angle of 22°, and a 0.5-mm-thick beryllium window. In this experiment, the tube voltage was from 45 to 65 kV, and the tube current was regulated to within 0.40 mA (maximum current) by the filament temperature. The exposure time is controlled in order to obtain optimum X-ray intensity. Monochromatic K$\alpha$ rays are selected out using a barium sulfate filter for absorbing bremsstrahlung and K$\beta$ rays. In designing the filter, the surface density of the barium sulfate powder is important, since the X-rays are absorbed effectively by the powder as compared with poly(methyl methacrylate) (PMMA) resin. In this case, the density was approximately 30 mg/cm$^2$.

## 3. Characteristics

### *3.1 X-ray intensity*

The X-ray intensity rate was measured by a Victoreen 660 ionization chamber at 1.0 m from the X-ray source (Fig. 3). At a constant tube current of 0.40 mA, the X-ray intensity increased when the tube voltage was increased. At a tube voltage of 60 kV and a current of 0.40 mA, the intensities without filtering and with the filter were 208 and 16.8 μGy/s, respectively, with errors of less than 0.2%. The X-ray intensity was limited because the thermal contact between the target and the anode was not good.

### *3.2 X-ray spectra*

In order to measure X-ray spectra, we employed a germanium detector (GLP-10180/07-P, Ortec Inc.) (Fig. 4). Without filtering, when the tube voltage was increased, the X-ray intensities of cerium K-series characteristic lines increased, and both the maximum photon energy and the bremsstrahlung X-ray intensity increased. Using the filter, both the K$\beta$ lines and the bremsstrahlung X-rays with photon energies higher than the barium K-edge of 37.4 keV were absorbed effectively, and sharp K$\alpha$ lines were left. With increases in the tube voltage, the K$\alpha$ intensity substantially increased, and the maximum photon energy increased.

In order to perform K-edge angiography, the K$\alpha$ rays are useful, and the high-energy bremsstrahlung X-rays decrease the image contrast. Using the filter, because bremsstrahlung X-rays with energies higher than 60 keV were not absorbed easily, the tube voltage for angiography was determined to be 60 kV. Subsequently, low-energy bremsstrahlung rays

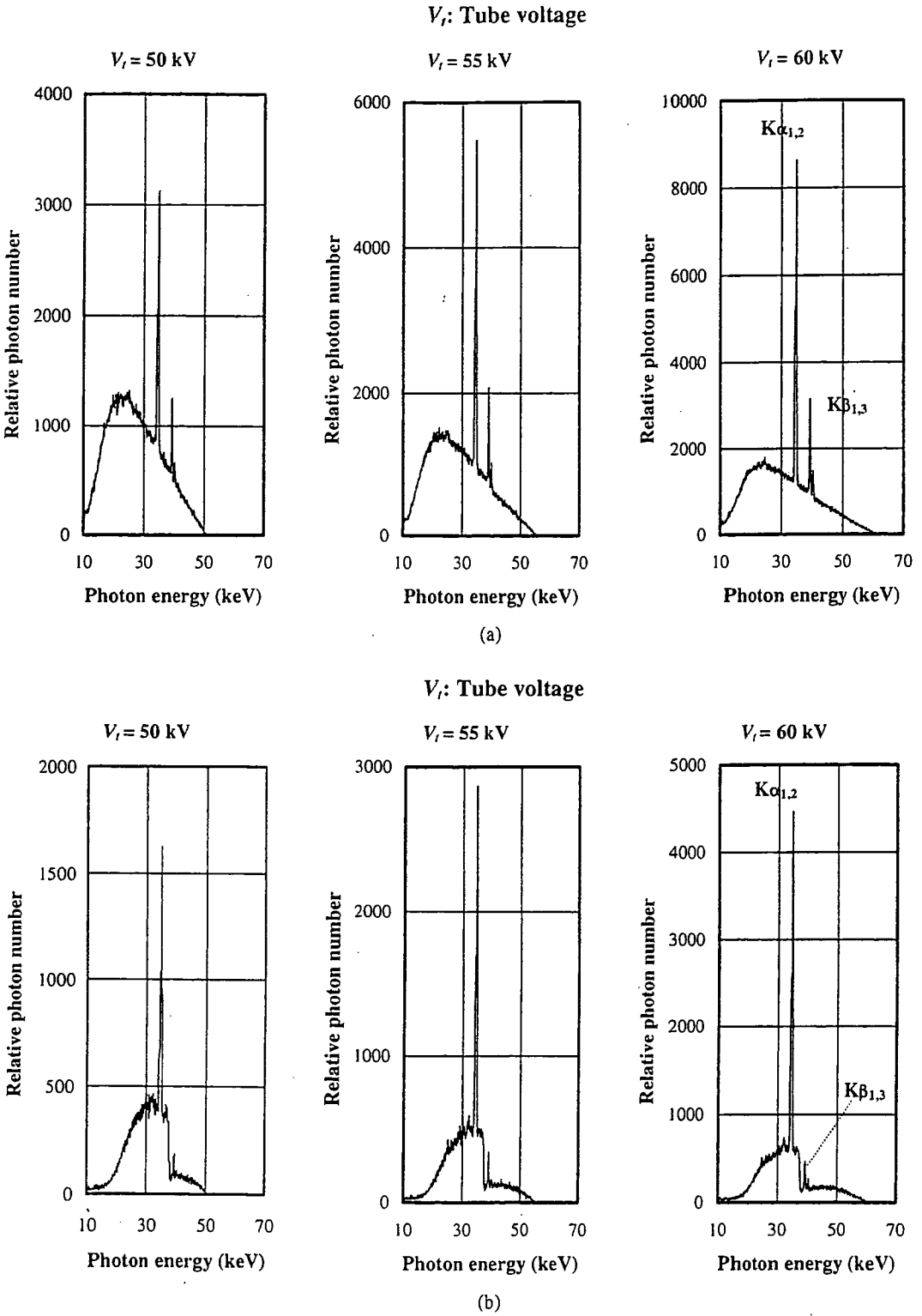


Fig. 4. X-ray spectra measured using germanium detector with changes in tube voltage (a) without filtering and (b) using barium sulfate filter.

with energies lower than the K-edge should be minimized using the filter or an aluminum filter to increase the blood-vessel contrast, since the iodine contrast media transmit the rays easily.

## 4. K-edge Angiography

Because the average photon energy of Kα is 34.6 keV, iodine contrast media with a K-absorption edge of 33.2 keV absorb the Kα lines easily. Therefore, blood vessels were observed with high contrasts. In order to observe fine blood vessels approximately 50 μm in diameter, the angiography was performed using an X-ray film (Fuji IX 100), iodine microspheres 15 μm in diameter, and the filter. The distance between the X-ray source and the imaging plate was 1.5 m, and the tube voltage was 60 kV. First, rough measurements of spatial resolution were made using wires. Figure 5 shows radiograms of tungsten wires coiled around rods made of PMMA with an X-ray exposure time of 300 s. Although the